isvr Institute of Sound and Vibration Research

Equipment Isolation of a SDOF System with an Inertial Actuator using Feedback Control Strategie – Part I: Theory

L. Benassi, P. Gardonio and S.J. Elliott

ISVR Technical Memorandum No 883

February 2002

University of Southampton

SCIENTIFIC PUBLICATIONS BY THE ISVR

Technical Reports are published to promote timely dissemination of research results by ISVR personnel. This medium permits more detailed presentation than is usually acceptable for scientific journals. Responsibility for both the content and any opinions expressed rests entirely with the author(s).

Technical Memoranda are produced to enable the early or preliminary release of information by ISVR personnel where such release is deemed to the appropriate. Information contained in these memoranda may be incomplete, or form part of a continuing programme; this should be borne in mind when using or quoting from these documents.

Contract Reports are produced to record the results of scientific work carried out for sponsors, under contract. The ISVR treats these reports as confidential to sponsors and does not make them available for general circulation. Individual sponsors may, however, authorize subsequent release of the material.

UNIVERSITY OF SOUTHAMPTON

INSTITUTE OF SOUND AND VIBRATION RESEARCH

SIGNAL PROCESSING AND CONTROL GROUP

Equipment Isolation of a SDOF System with an Inertial Actuator using Feedback Control Strategies - Part I: Theory

by

L. Benassi, P. Gardonio and S. J. Elliott

ISVR Technical Memorandum No. 883

February 2002

Authorised for issue by
Prof S J Elliott
Group Chairman

ABSTRACT

Vibration isolators are required to protect a delicate piece of equipment from the vibration of a structure to which it is attached. This report describes a theoretical investigation into an active vibration isolation system in which an electromagnetic inertial actuator is installed on top of a piece of equipment which is connected to a vibrating base structure through a passive mount. Several feedback control schemes are discussed, and simulation results are reported.

In addition, low and high frequency stability issues are investigated. Sensors and actuators together with associated signal conditioning equipment play an important role in active vibration control, but often place limits on the control performance. It is discussed how electronic components, which are a major source of instability, make an unconditionally stable system into a conditionally stable one.

TABLE OF CONTENTS

1. INTRODUCTION

Isolators are generally required to protect a piece of delicate equipment in a severe vibration environment.
Very little can often be done to reduce the base vibration since it is either of high impedance or characterized by complex dynamics. The isolation of any vibration-sensitive equipment from base vibration is therefore usually performed on the transmission paths (mounts). The fundamental benefit provided by any mount is reduced structural vibration. In many applications, unwanted noise is a direct result of structural vibrations. Therefore, mounts also provide noise reduction benefits. In general, these mounts may be modelled as a combination of both resilient and energy dissipating elements. However, with such passive mounts there is a trade-off between low and high frequency isolation performances depending on the damping of the mount. In fact, a major challenge is to make the mount as stiff as possible, statically, to better support the equipment, and dynamically as soft as possible, to better isolate it. This is difficult to accomplish with passive elastometric mounts, as described by Crede and Ruzicka (1996) and Ungar (1992). To provide a more favourable static and dynamic stiffness compromise, active isolation solutions must be used, which are usually based on mounts and actuators.
Applications with actuators and passive mounts in an active isolator package provide many benefits including simplicity, effective vibration isolation, noise attenuation, higher static stiffness, dynamic adaptability, and safety. This suggests that there is ample motivation for the use of active mounting systems.

A very large number of published papers have been concerned with vibration isolation problems and feedback active vibration control methods have been discussed. Karnopp (1995) proposed a velocity feedback control method for obtaining a non-resonant response, which has been applied to various vibration isolation systems.
Position feedback makes the rigidity increase and the transmissibility decrease, as investigated by Bhat (1991). However, to have zero transmissibility, the rigidity must be infinite, so the feedback coefficient must be infinite. Hence it is impossible to have zero transmissibility by using the usual feedback control methods.

One way of overcoming the trade-off between damping low-frequency resonances and achieving good high-frequency isolation is thus to use skyhook damping. This was investigated by Beard, von Flotow and Schubert (1994). In their study, skyhook damping implementation was possible using reactive actuators since no base dynamics were taken into account in the frequency range of control, so that an inertial ground was available. The effect of skyhook damping has also been investigated for a finite mobility base (Kim, Elliott and Brennan, 1999) using reactive actuators.

In the study by Serrand et al. (1998 and 2000), the effect of the base structure dynamics on the formulation of direct velocity feedback (DVFB) control was investigated. In the case of a reactive implementation of the control actuators, the secondary forces were generated by reacting off the flexible base structure, therefore the classical model of perfect skyhook damping was not valid and the inherent stability of DVFB control (Balas, 1978) had to be reconsidered. It was found that no instability or vibration amplification was encountered from potential re-excitation of the flexible base by the secondary actuators in the frequency range of analysis. Moreover, changes in the dynamics of the base plate did not destabilize the control system, illustrating its robustness.

On the other hand, considering the effects of the equipment and the mounts on the stability of the overall system, there are severe limitations. In theory, DVFB is unconditionally stable, provided the equipment can be modelled as a rigid body and the mounts as a lumped parameter spring and dampers. In practice, instability occurred at a very low frequency due to phase shifts of the electrical equipment used, the flexibility in the equipment structure, and the effect of resonances in the mount.

Actuators are used in active vibration control to generate a secondary vibrational response, and in practice they can be configured either to react off the base structure or function as an inertial actuator (also called proof-mass actuator.) This was investigated by Elliott *et al.*, (2001). This choice also influences the stability limit. In general, the design of a feedback controller involves a trade-off between performance (the attenuation of the disturbance) and robust stability (the ability to remain stable under changing conditions).

The impedance and mobility matrices approach (IMM) was employed in this study. Recent studies on active isolation by Gardonio et al. (1997a, 1997b, 1998) have suggested the need for mathematical models which give a detailed analysis of the coupled vibration transmission mechanism and, at the same time, provide a summary of the overall phenomenon and thus allow a global interpretation of the dynamics of the active isolator system. Good results have been obtained by using the IMM approach where the system is divided into individual components and each component is studied in terms of input and transfer mobilities or impedances.

This report deals with the stability analysis of a single degree of freedom system, composed of a piece of equipment, which is mounted on a vibrating mass through a mount. Active control is performed through an inertial actuator.

2. ACTIVE ISOLATION OF A LUMPED MASS EQUIPMENT MOUNTED ON A SPRING-DASHPOT-MASS BASE VIA A SPRING-DASHPOT MOUNT

In this study, a matrix model has been used which assumes that the system is divided into four elements: the vibrating base, the passive mounts, the equipment, and the inertial actuator. The dynamics of each of these elements modelled as lumped systems is evaluated using point mobility terms. Fig. 1 shows the typical system that has been used in the first section of this study and the numerical values assumed for the simulations. With these values the base has a natural frequency of about 1.75 Hz and a damping ratio of about ζ=0.5%, the actuator has a natural frequency of about 10 Hz and a damping ratio of about ζ=4.5%, and the equipment mount has a natural frequency of about 21.5 Hz and a damping ratio of about ζ=5.2%.

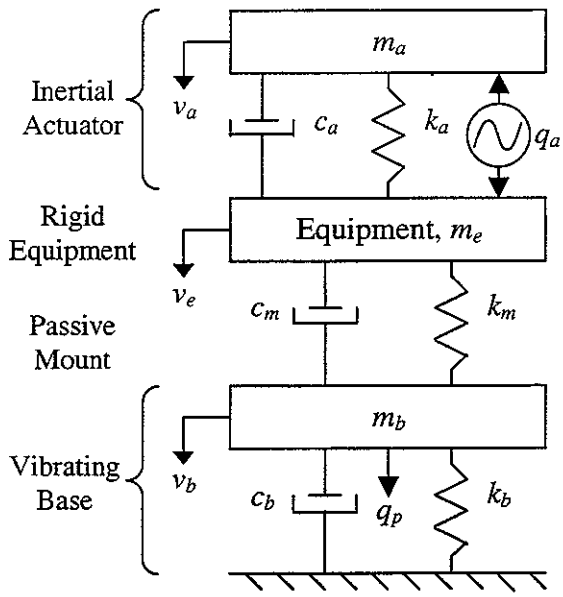

m_a = Inertial Actuator Dynamic Mass = 0.91 Kg
c_a = Inertial Actuator Damping Factor = 5.8 Ns/m
k_a = Inertial Actuator Spring Stiffness = 3900 N/m
m_e = Equipment Mass = 2.9 Kg
c_m = Passive Mount Damping Factor = 33 Ns/m
k_m = Passive Mount Spring Stiffness = 48000 N/m
m_b = Base Mass = 2900 Kg
c_b = Base Damping Factor = 330 Ns/m
k_b = Base Spring Stiffness = 112000 N/m

q_p = Primary Force (disturbance)
q_a = Secondary Force (control)
v_a = Inertial Actuator Velocity
v_e = Equipment Velocity
v_b = Base Velocity

Fig. 1 *Schematic of a vibration isolation system with an inertial actuator.*

The following definitions of mobilities and impedances have been used to describe the system throughout this work:

$$Y_a = \frac{1}{j\omega m_a} = \text{Mobility of the actuator mass} \tag{2.1}$$

$$Y_e = \frac{1}{j\omega m_e} = \text{Mobility of the rigid equipment} \tag{2.2}$$

$$Y_b = \frac{1}{j\omega m_b + c_b + \frac{k_b}{j\omega}} = \text{Mobility of the vibrating base} \tag{2.3}$$

$$Z_a = c_a + \frac{k_a}{j\omega} = \text{Impedance of the actuator damping and stiffness} \tag{2.4}$$

$$Z_m = c_m + \frac{k_m}{j\omega} = \text{Impedance of the passive mount} \tag{2.5}$$

$$A = \frac{j\omega m_a}{Z_a + j\omega m_a} = \text{Total force on the equipment per } q_a \text{ when } v_e = 0 \quad (2.6)$$

$$B = \frac{j\omega m_a Z_a}{Z_a + j\omega m_a} = \text{Impedance of the total force on the equipment per } v_e \text{ when } q_a = 0 \quad (2.7)$$

2.1 Velocity Feedback Control with Inertial Actuators

The analytic equation that describes the influence of the primary and secondary excitations on the sensor output, which is the equipment velocity, can be shown to be

$$v_e = \frac{Y_e A(1 + Y_b Z_m)}{1 + Z_m(Y_e + Y_b + Y_e B Y_b) + Y_e B} q_a + \frac{Y_e Y_b Z_m}{1 + Z_m(Y_e + Y_b + Y_e B Y_b) + Y_e B} q_p \quad (2.8)$$

or

$$v_e = G_v q_a + G_{dv} q_p \quad (2.9)$$

where G_v is the plant and G_{dv} is the disturbance due to the primary excitation. When DVFB, described by

$$q_a = -h_v v_e \quad (2.10)$$

is used to control the equipment velocity as in Fig. 2, the corresponding Bode plot of the plant is reported in Fig. 3. The Nyquist plot (Fig. 4) shows a portion of the curve at low frequency which lies on the negative side of the x-axis, and the correspondent root locus (Fig. 5) shows how the poles and zeros of the system behave when the feedback gain h_v varies from 0 to $+\infty$. In particular the real part of the actuator complex conjugate poles become positive when h_v = 58 leading the system in the unstable region. Note that the base resonance is so low that it does not significantly alter the system stability. Substituting (2.10) into (2.8), the closed loop behaviour can be written as

$$v_e = \frac{Y_e Y_b Z_m}{1 + Z_m(Y_e + Y_b + Y_e B Y_b) + Y_e B + Y_e A(1 + Y_b Z_m) h_v} q_p \quad (2.11)$$

The transmissibility of the system (Fig. 6), defined as the ratio between equipment velocity and base velocity, is given by

$$\frac{v_e}{v_b} = \frac{Y_e Z_m}{1 + Z_m Y_e + Y_e B + Y_e A h_v} \quad (2.12)$$

When h_v is set to zero, (2.12) provides the transmissibility of the system without control (passive system.) In Fig. 6, for gains below the critical point, the attenuation does not seem to be pronounced. In particular, when the gain is set to 57, the maximum attenuation is about 8 dB, while the average attenuation within the 15-25 Hz frequency range, is about 3 dB. In sum, the implementation of DVFB control leads to a trade-off between performance and stability.

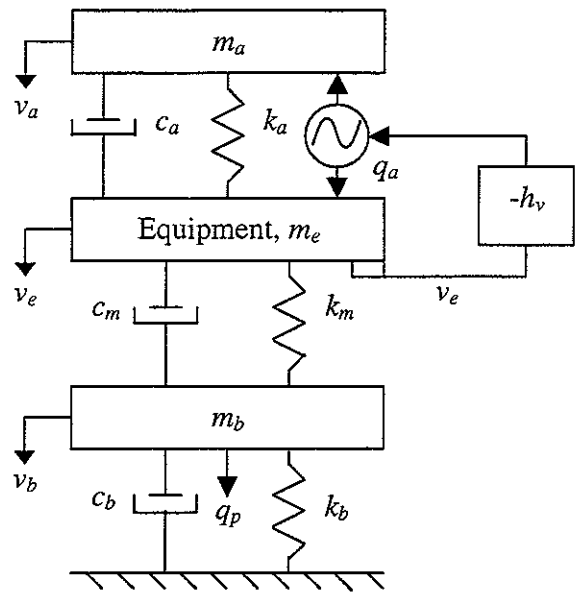

Fig. 2 *Schematic of a vibration isolation system with an inertial actuator and equipment velocity feedback control.*

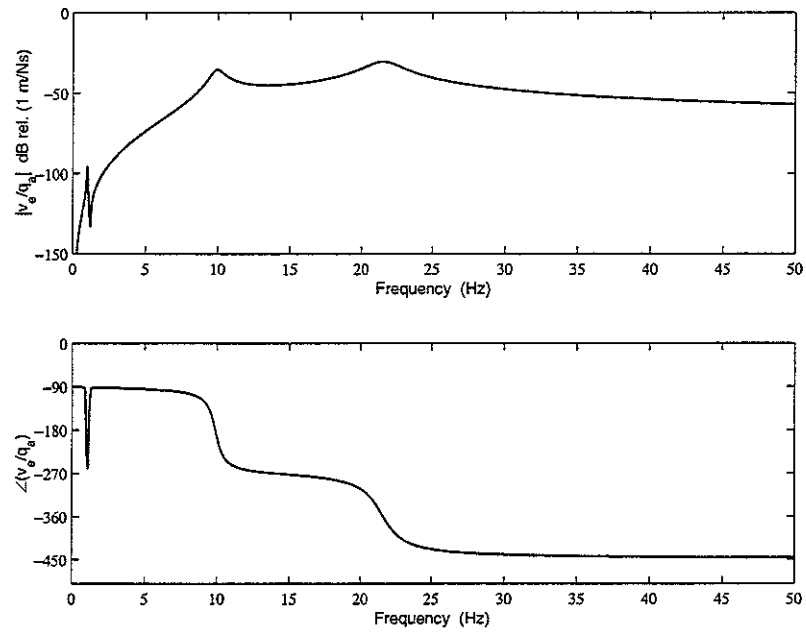

Fig. 3 *Bode plot of the equipment velocity per secondary excitation of a vibration isolation system with an inertial actuator and velocity feedback control.*

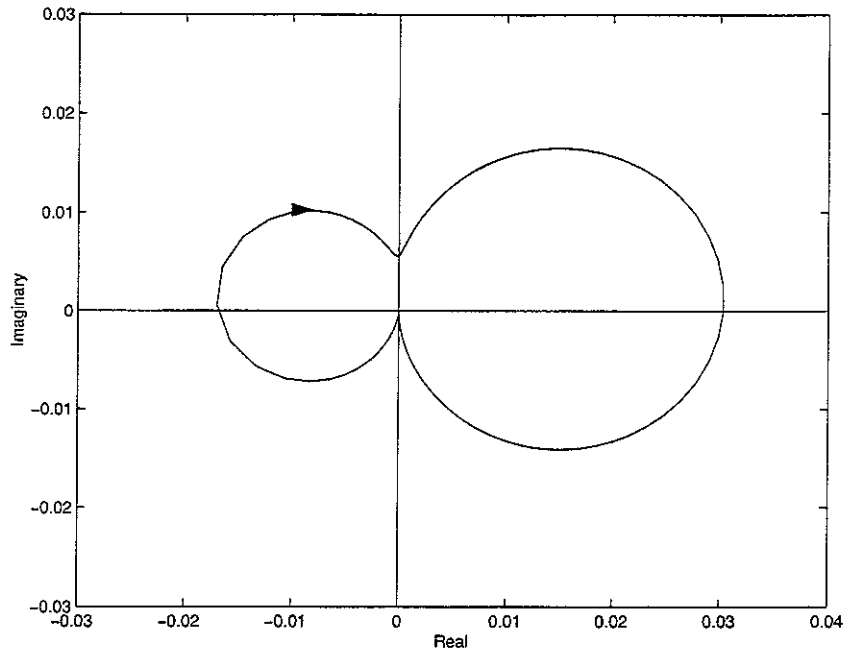

Fig. 4 *Nyquist plot of the transfer function between secondary excitation and equipment velocity of a vibration isolation system with an inertial actuator and velocity feedback control. ω varies from 0 to $+\infty$.*

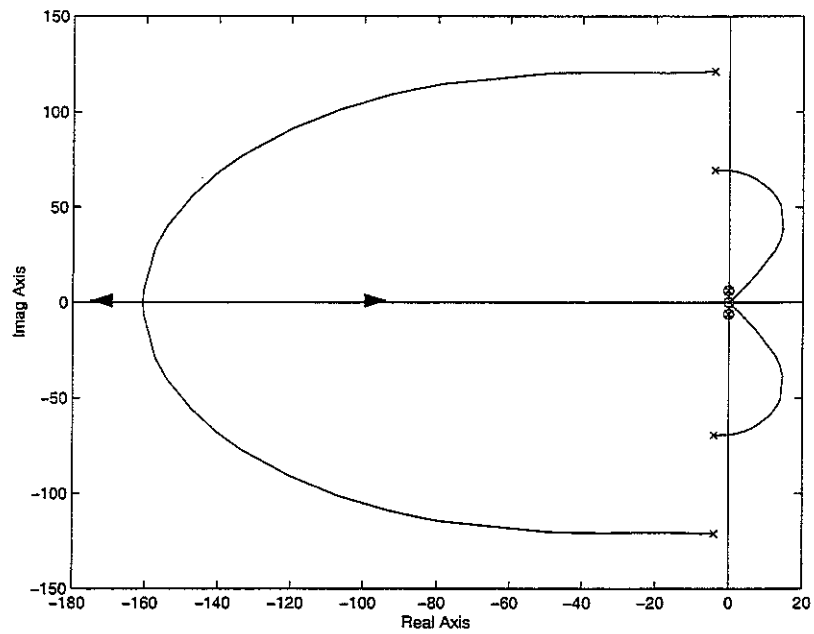

Fig. 5 *Root locus of the transfer function between secondary excitation and equipment velocity of a vibration isolation system with an inertial actuator and velocity feedback control. Note that the base dynamics becomes unstable for very large gains.*

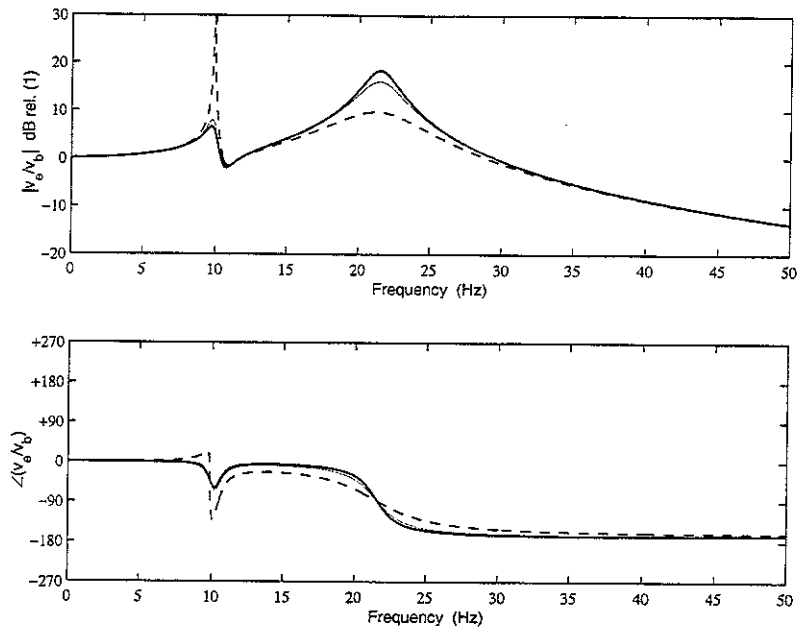

Fig. 6 *Transmissibility of a vibration isolation system with an inertial actuator and velocity feedback control. Velocity feedback gain h_v = 0 (bold line), h_v = 10 (faint line), h_v = 57 (dashed line.) The higher the gain, the more energy is taken away from the structure. However, the higher the gain, the closer to instability the actuator mode is.*

The second part of this memorandum presents a review of different strategies for active isolation (Miu, 1993, Preumont, 1997 and 2001, Howard and Hansen, 1997) using inertial actuators. Six alternative control strategies have been considered: integrated velocity feedback control, force control, integrated force control, force and velocity control, integrated force and velocity control, and integrated force and integrated velocity control. The purpose of this section is to study the feedback stability limits of the different control strategies, paying attention to their closed loop performance and robust behaviour.

2.2 Integrated Velocity Feedback Control

When the feedback gain h_v is replaced with an integrator, the feedback stability of the closed loop system is then dramatically improved (Fig. 7.) This is better illustrated by the Nyquist plot in Fig. 8 and the root locus in Fig. 9. In this study the transfer function of the controller was chosen to be

$$H(j\omega) = \frac{h_{iv}}{j\omega} \tag{2.13}$$

Considering (2.8) as the open loop response, by feeding back

$$q_a = -H(j\omega)v_e \tag{2.14}$$

the following closed loop transfer function is obtained:

$$v_e = \frac{Y_e Y_b Z_m}{1 + Z_m(Y_e + Y_b + Y_e B Y_b) + Y_e B + Y_e A(1 + Y_b Z_m) H(j\omega)} q_p \qquad (2.15)$$

while the transmissibility is given by

$$\frac{v_e}{v_b} = \frac{Y_e Z_m}{1 + Z_m Y_e + Y_e B + Y_e A H(j\omega)} \qquad (2.16)$$

This is illustrated in Fig. 10. Although high gains might be required, the integrated velocity feedback controller provides a very good attenuation not only about the inertial actuator frequency, but also within a considerable frequency range, which also includes the base-equipment structural mode. In particular, for h_{iv}=1000, the average attenuation within the frequency range 7 Hz to 27 Hz is over 20 dB.
Expanding (2.16), it can be noted that the zero (anti-resonance) of the system is not affected by h_{iv}, while the actuator-dominated resonance (pole) and the structure-dominated resonance are. In particular, h_{iv} acts directly on m_a . Therefore, when h_{iv} increases, the actuator-dominated resonance decreases. At the same time, h_{iv} acts on the stiffness of the structure-dominated resonance, so when h_{iv} increases, this latter resonance increases. This behaviour is also shown in fig. 10.

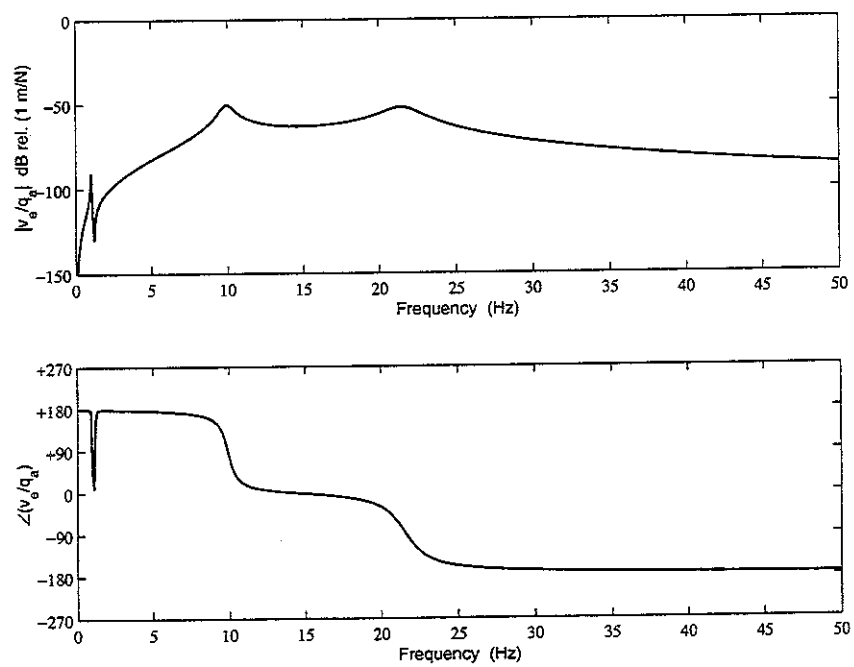

Fig. 7 *Bode plot of the equipment velocity per secondary excitation followed by an integrator of a vibration isolation system with an inertial actuator and integrated feedback control. The open loop transfer function $G(j\omega)H(j\omega)$ is reported.*

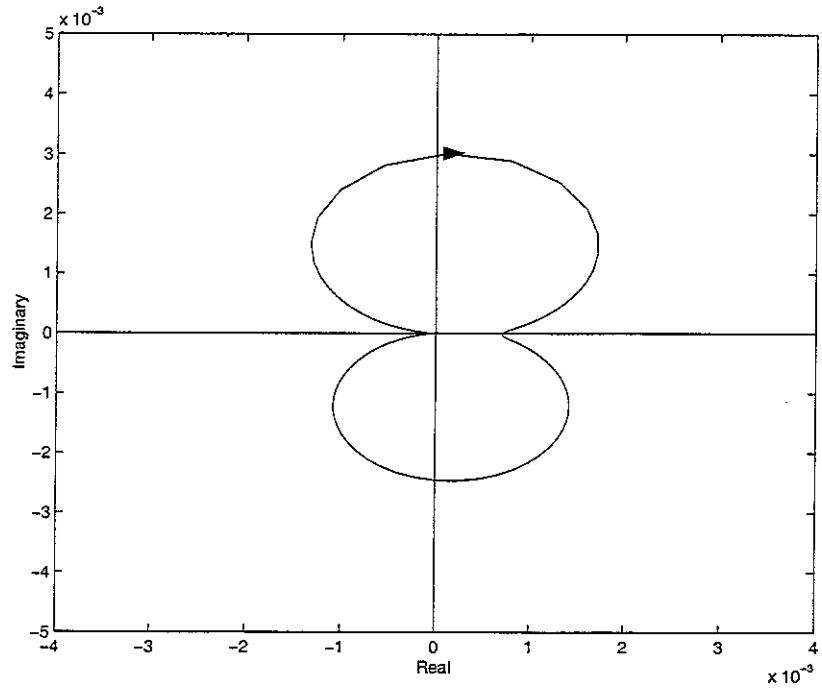

Fig. 8 *Nyquist plot of the transfer function between secondary excitation and equipment velocity followed by an integrator of a vibration isolation system with an inertial actuator and integrated feedback control. ω varies from 0 to $+\infty$.*

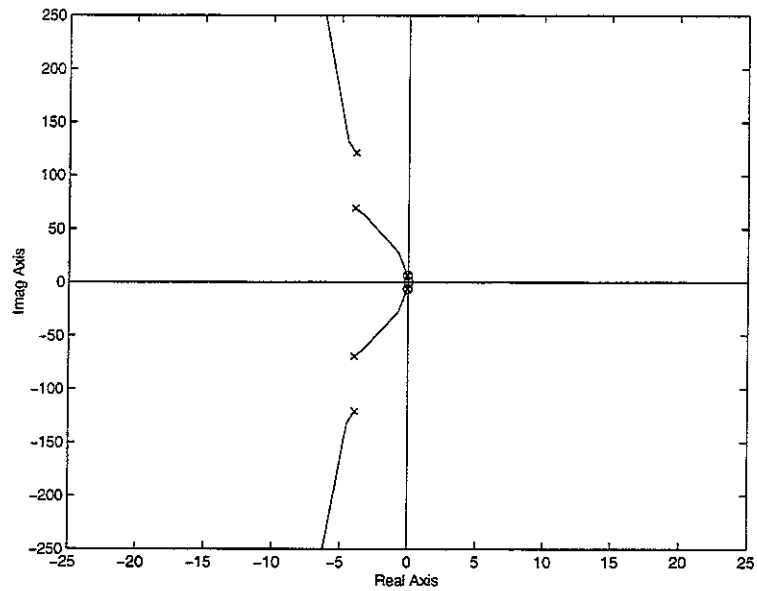

Fig. 9 *Root locus of the transfer function between secondary excitation and equipment velocity of a vibration isolation system with an inertial actuator and integrated feedback control.*

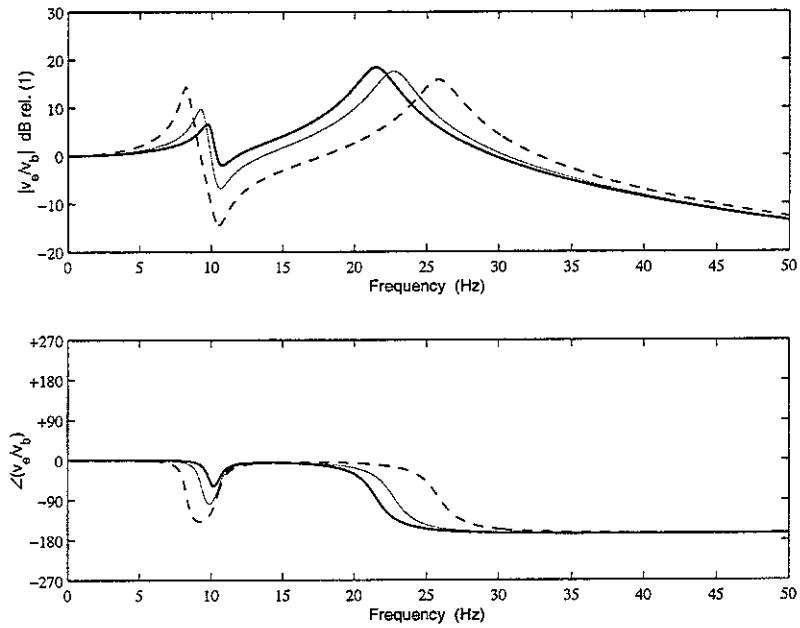

Fig. 10 *Transmissibility of a vibration isolation system with an inertial actuator and integrated velocity feedback control. Integrator gain h_{iv} = 0 (bold line), h_{iv} = 10 (faint line), and h_{iv} = 1000 (dashed line.)*

The closed loop system is unconditionally stable for any feedback gain h_{iv}. This is true only for ideal integrators. In fact, when the pole of the integrator is not exactly zero, the derivative of the Nyquist plot about ω=0 is not zero, but it is positive. Therefore, from ω=0, the Nyquist plot initially starts in the third quadrant. This means that the curve encircles the point (-1,0) for h_{iv} greater than a certain critical value. In other words, for real integrators, the system becomes conditionally stable. In this case, in the root locus the complex conjugate poles relative to the inertial actuator cross the imaginary axis, rather than staying on the negative side of the x-axis. Also, high frequency causes of instability may affect the overall system.

A robust analysis on the system with integrated feedback shows how sensitive the closed loop system is with respect to some of the most common causes of high and low frequency instability. In real systems many other components are present in the control loop (Ananthaganeshan, 2001, and Ren, *et al.*, 1997.) Fig. 11 illustrates a more realistic block diagram for a real system based on integrated control. Accelerometers are very common vibration transducers, and their output is often amplified by a charge amplifier, which behaves like a high-pass filter. If velocity is needed, the measured signal must be integrated. Ideal integrators do not exist, therefore their dynamics must be taken into account in the overall stability analysis. In the control segment of the loop, after the controller, a power amplifier is usually employed to amplify the signal and make it appropriate for the actuator. Also, a delay is usually present, mostly due to transmission lags of the electric signal.

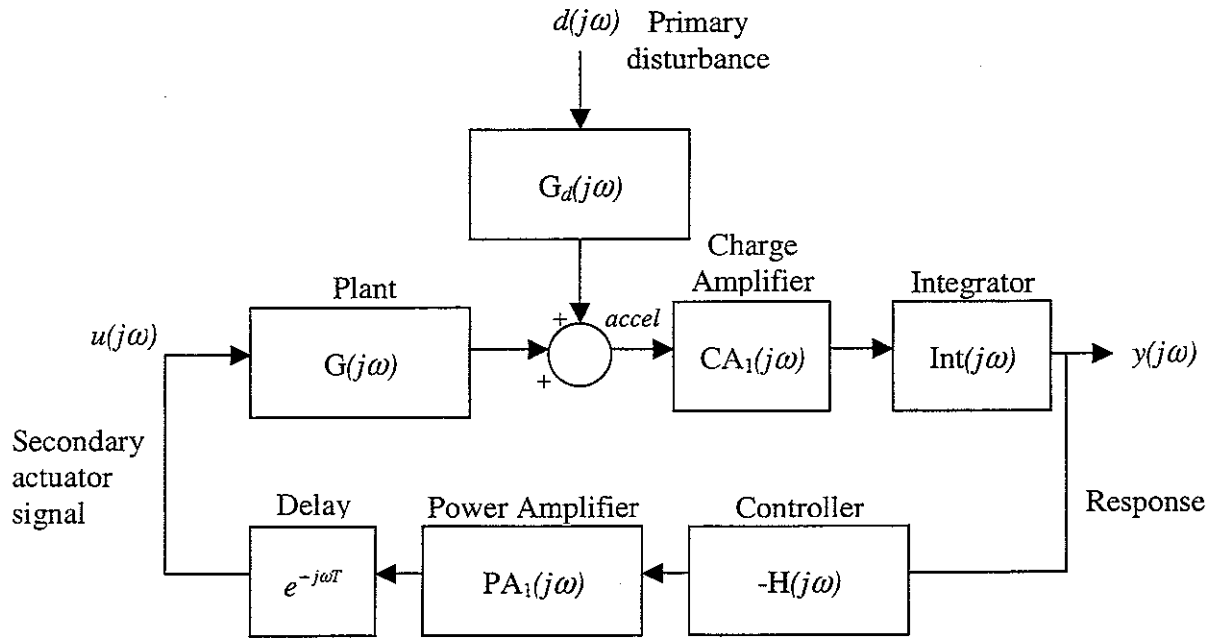

Fig. 11 *Block diagram of a realistic negative feedback control system including the plant, the integrated controller, and the electronic components.*

The following equations illustrate the dynamics of the components in Fig. 11. The numerical values have been chosen according to off-the-shelf commercial components currently used in the laboratory. In particular, the charge amplifier cut-off frequency is 1 Hz. In the case subject of this study, the plant is different from (2.8) because in this case its output is acceleration, not velocity. The controller is composed of a second order high-pass filter and an integrator:

$$G(j\omega) = \frac{j\omega Y_e A(1 + Y_b Z_m)}{1 + Z_m(Y_e + Y_b + Y_e B Y_b) + Y_e B} \tag{2.17}$$

$$H(j\omega) = \frac{-\omega^2 0.1326}{(1 + j\omega 0.1326)^2} \cdot \frac{h_i}{1 + j\omega 0.0909} \tag{2.18}$$

$$CA_1(j\omega) = \frac{j\omega 0.159}{1 + j\omega 0.159} \tag{2.19}$$

$$Int(j\omega) = \frac{1}{1 + j\omega 0.251} \tag{2.20}$$

$$PA_1(j\omega) = \frac{j\omega 0.1326}{1 + j\omega 0.1326} \tag{2.21}$$

The open loop frequency response function of the system shown in Fig. 11 can be written as

$$G\ (j\omega)H_t(j\omega) = G(j\omega)CA_1(j\omega)Int(j\omega)H(j\omega)PA_1(j\omega)e^{-j\omega T} \tag{2.22}$$

while the closed loop frequency response function is given by

$$v_e = \frac{G_d(j\omega)}{1+G(j\omega)H_t(j\omega)} q_p \tag{2.23}$$

where

$$G_d = \frac{j\omega Y_e Y_b Z_m}{1+Z_m(Y_e+Y_b+Y_e B Y_b)+Y_e B} \tag{2.24}$$

A description of the effects of the main causes of instability is given in Benassi (2001). In particular, the overall frequency response of all the electronic components, given by

$$G_{ec}(j\omega) = CA_1(j\omega)Int(j\omega)H(j\omega)PA_1(j\omega)e^{-j\omega T} \tag{2.25}$$

is reported in Fig. 12.

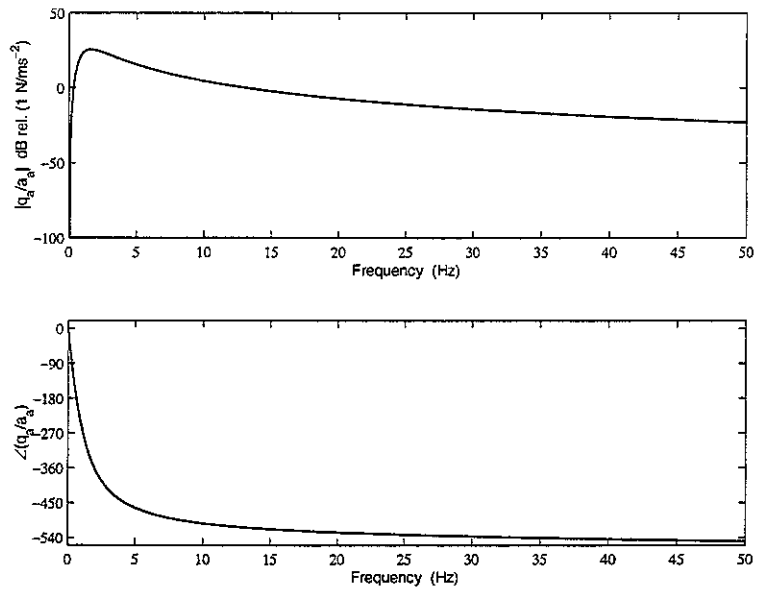

Fig. 12 *Bode plot of the overall frequency response of all the electronic components.*

Given the realistic system in Fig. 11, described by (2.17) through (2.24), and also assuming a time delay T=0.001 seconds, the maximum gain h_{iv} that guarantees the system to be stable is 22. This is illustrated in Fig. 13. For this value of the feedback gain, the maximum attenuation in the closed loop response (Fig. 14) is computed to be 6 dB, while the average attenuation between the two main resonance frequencies is 3 dB.
At the critical point (-1,0), the frequency value that the Nyquist plot assumes is 9.4 Hz.

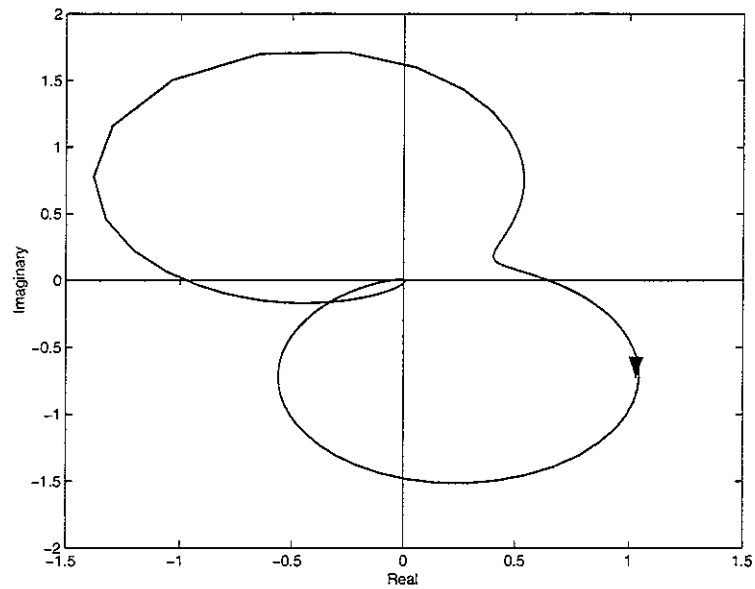

Fig. 13 *Nyquist plot of the transfer function between secondary excitation and equipment velocity of a realistic vibration isolation system with an inertial actuator and integrated feedback control. Realistic electronic components are used, the delay is assumed to be 0.01 seconds, and the feedback gain is set to 22. ω varies from 0 to $+\infty$.*

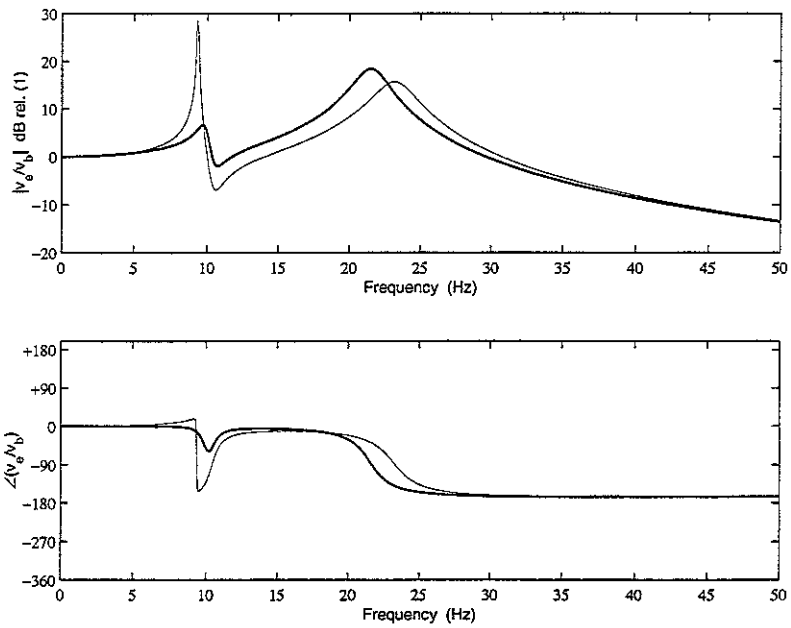

Fig. 14 *Transmissibility of the ideal system without control (solid line) and the realistic (faint line) vibration isolation system with an inertial actuator and integrated velocity feedback control. Realistic electronic components are simulated, the delay is assumed to be 0.01 seconds, and the feedback gain is set to 22.*

2.3 Force Feedback Control

Applying force feedback control to the original system is the next logical step. Fig. 15 shows the implementation. The total force q_t is measured by a force gauge, which is located between the inertial actuator and the equipment. This signal is then multiplied by the feedback gain h_f and fed back to the secondary excitation. The system equation is given by

$$q_t = \frac{A(1+Z_m(Y_b+Y_e))}{1+Z_m(Y_e+Y_b+Y_eBY_b)+Y_eB}q_a + \frac{Y_eY_bZ_mB}{1+Z_m(Y_e+Y_b+Y_eBY_b)+Y_eB}q_p \quad (2.26)$$

or

$$q_t = G_f q_a + G_{df} q_p \quad (2.27)$$

where G_f is the plant and G_{df} is the disturbance due to the primary excitation. The control law is specified by

$$q_a = -h_f q_t \quad (2.28)$$

The corresponding Bode plot (Fig. 16) shows the inertial actuator mode at 11 Hz, and then the passive isolation system behaviour at about 22 Hz. In this ideal case, the closed loop system is unconditionally stable, as illustrated by the Nyquist plot (Fig. 17) and the root locus (Fig. 18.)
Recalling the possible causes of instability, a potential instability at low frequency due to phase shifts of the electronic devices may occur. In the ideal case the derivative at $\omega = 0$ is zero, but in real systems it might be positive, compromising the robustness of the overall system and making it conditionally stable.

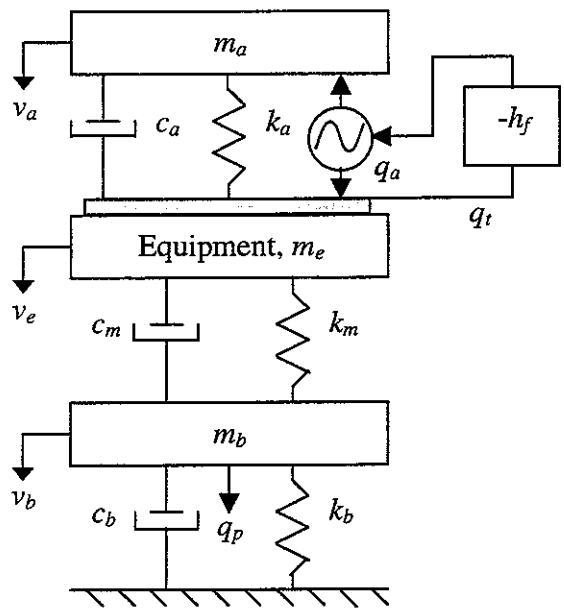

Fig. 15 *Schematic of a vibration isolation system with an inertial actuator and force feedback control.*

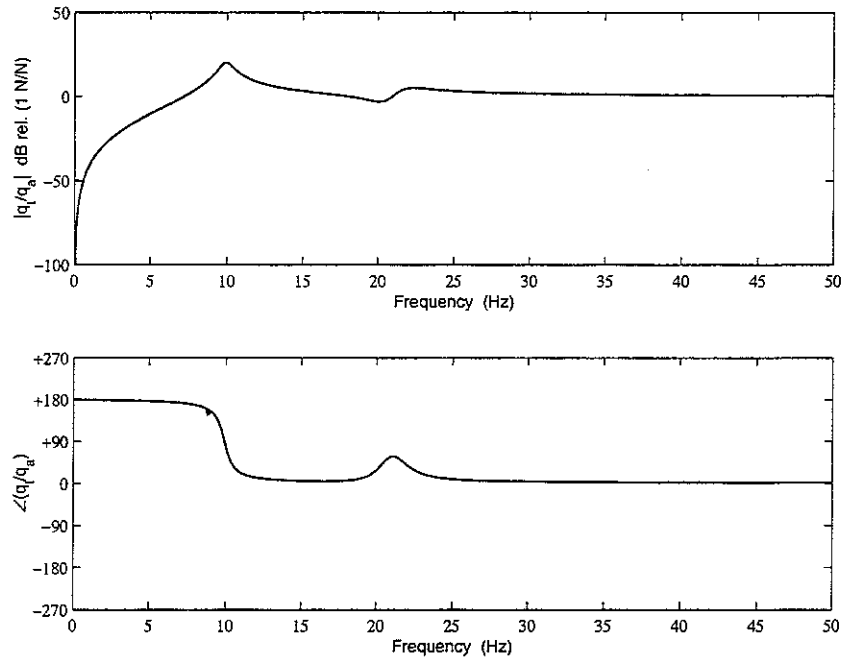

Fig. 16 *Bode plot of the total measured force per secondary excitation of a vibration isolation system with an inertial actuator and force feedback control.*

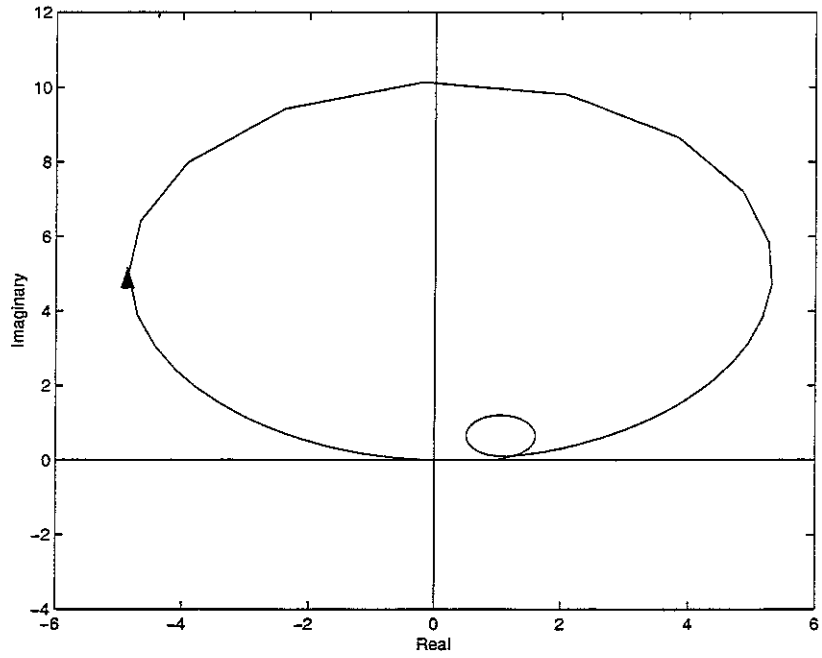

Fig. 17 *Nyquist plot of the transfer function between secondary excitation and total measured force of a vibration isolation system with an inertial actuator and force feedback control. ω varies from 0 to $+\infty$.*

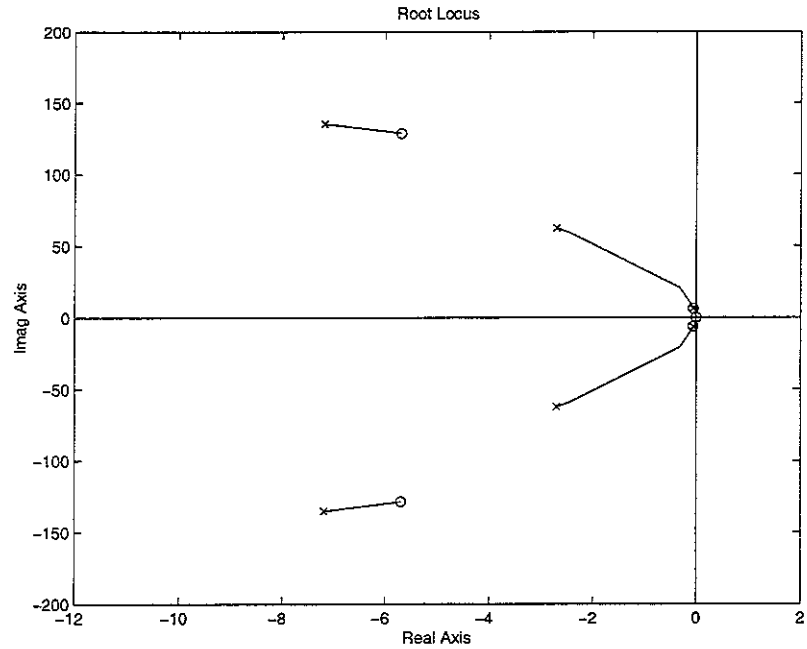

Fig. 18 *Root locus of the transfer function between secondary excitation and total measured force of a vibration isolation system based on an inertial actuator and force feedback control. Note that the base dynamics becomes unstable for very large gains.*

By substituting (2.28) into (2.26) the following is obtained. It describes the influence of the primary excitation on the measured signal (Fig. 19.)

$$q_t = \frac{Y_e Y_b Z_m B}{1 + Z_m(Y_e + Y_b + Y_e B Y_b) + Y_e B + A(1 + Z_m(Y_b + Y_e))h_f} q_p \tag{2.29}$$

Similarly,

$$q_t = \frac{B}{1 + Ah_f} v_e = \frac{j\omega m_a k_a - \omega^2 m_a c_a}{k_a + j\omega c_a - \omega^2 m_a (1 + h_f)} v_e \tag{2.30}$$

and this is shown in Fig. 20. The transmissibility is given by

$$\frac{v_e}{v_b} = \frac{Y_e Y Z_m (1 + Ah_f)}{1 + Z_m Y_e + Y_e B + A(1 + Z_m Y_e)h_f} \tag{2.31}$$

The very interesting effect of the analysed force feedback controller is to be able to move the actuator resonance to lower frequencies, while its magnitude increases. This is not the only result. In fact, by examining the total measured force per primary excitation, the second outstanding result is the considerable force attenuation that this control offers at frequencies higher than the inertial actuator mode. Thirdly, when h_f increases, the structure-dominated resonance decreases. When, h_f tends to infinity, the structure-dominated resonance tends to a frequency which would be the resonance on an equivalent system in which m_a and m_e are joined together.

The physical interpretation of the force feedback control can be understood by analysing the system from a different point of view. By feeding back the inertial actuator acceleration, the behaviour of the closed loop system is identical to the behaviour of the closed loop system when force feedback control is applied (Benassi, 2001) In particular, it is found that, when $h_f = m_a\ h_a$, the two systems are equivalent, where h_a is the inertial actuator acceleration gain. This leads to the conclusion that force feedback control has the physical meaning of adding an "apparent" mass to the inertial actuator mass. Therefore, at higher frequencies than the inertial actuator resonance, the system appears to be more massive.

For high gains, the actuator resonance frequency becomes smaller than the first mode of the system (due to the base). In this configuration its amplitude is very small and the system is very well damped throughout the entire frequency spectrum. However, the problem of obtaining such high gains in practice remains.

Fig. 21 shows the transmissibility of the system. It can be noted that there is amplification of the equipment velocity. Since the aim of this study is to minimize the equipment velocity, this strategy seems to be counterproductive.

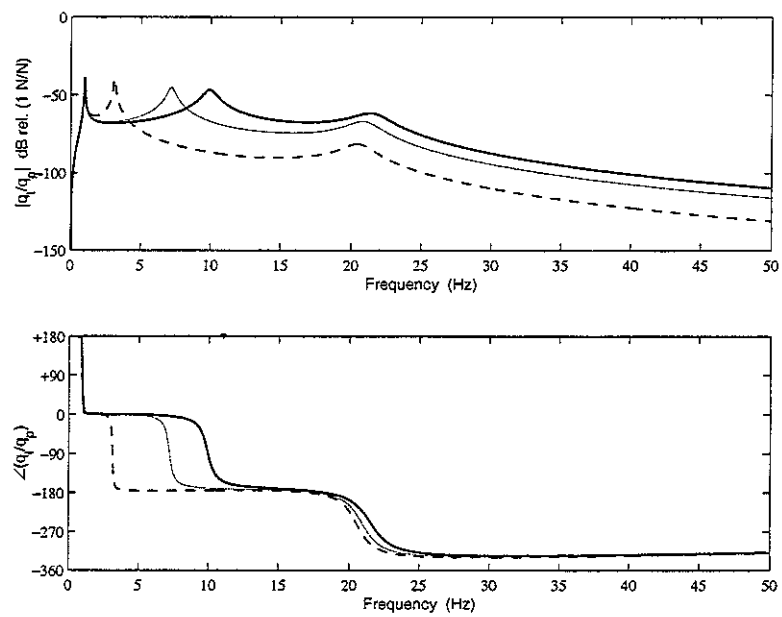

Fig. 19 *Bode plot of the transfer function between primary excitation and total measured force of a vibration isolation system with an inertial actuator and force feedback control. Three force feedback gains h_f have been analysed: $h_f = 0$ (bold line), $h_f = 1$ (faint line), and $h_f = 10$ (dashed line.)*

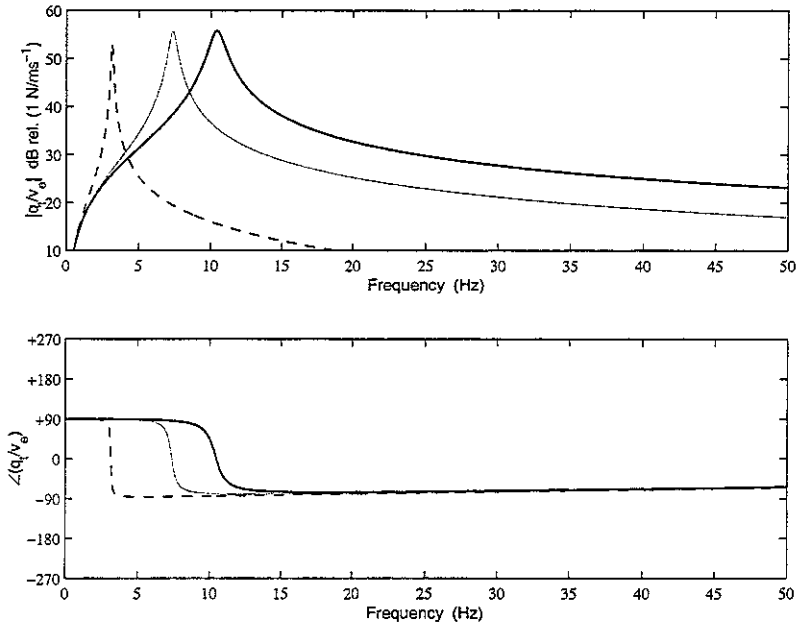

Fig. 20 *Bode plot of the transfer function between equipment velocity and total measured force of a vibration isolation system with an inertial actuator and force feedback control. Three force feedback gains h_f have been analysed: h_f = 0 (bold line), h_f = 1 (faint line), and h_f = 10 (dashed line.)*

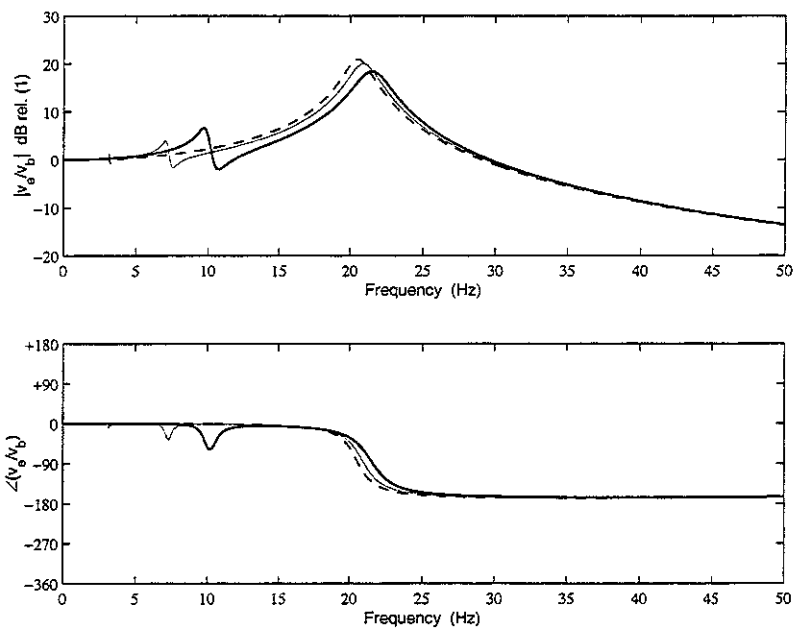

Fig. 21 *Bode plot of the transfer function between primary velocity and equipment velocity (transmissibility) of a vibration isolation system with an inertial actuator and force feedback control. Three force feedback gains h_f have been analysed: h_f = 0 (bold line), h_f = 1 (faint line), and h_f = 10 (dashed line.)*

In real systems based on force control, unlike the integrated control solution, the force gauge measurement does not need to be integrated. In other words, the charge amplifier and the integrator of Fig. 11 are replaced by a slightly different charge amplifier described by (2.30). The following equations illustrate the dynamics of the components:

$$G(j\omega) = \frac{A(1 + Z_m(Y_b + Y_e))}{1 + Z_m(Y_e + Y_b + Y_e B Y_b) + Y_e B} \tag{2.32}$$

$$H(j\omega) = \frac{-\omega^2 h_f 0.1326}{(1 + j\omega 0.1326)^2} \tag{2.33}$$

$$CA_2(j\omega) = \frac{j\omega 0.2385}{1 + j\omega 0.2385} \tag{2.34}$$

$$PA_1(j\omega) = \frac{j\omega 0.1326}{1 + j\omega 0.1326} \tag{2.35}$$

The open loop frequency response function of the system can be written as

$$G(j\omega)H_t(j\omega) = G(j\omega)CA_2(j\omega)H(j\omega)PA_1(j\omega)e^{-j\omega T} \tag{2.36}$$

while the closed loop frequency response function is given by

$$v_e = \frac{G_d(j\omega)}{1 + G(j\omega)H_t(j\omega)} q_p \tag{2.37}$$

where

$$G_d(j\omega) = \frac{Y_e Y_b Z_m B}{1 + Z_m(Y_e + Y_b + Y_e B Y_b) + Y_e B} \tag{2.38}$$

A quantitative performance comparison is now performed. Given the realistic system described by (2.32) to (2.38), and also assuming a time delay T=0.001 seconds, the maximum gain h_f that guarantees the system to be stable is 0.036. This is illustrated in Fig. 22. For this value of the gain, the maximum attenuation of the transmitted force in the closed loop response (Fig. 23) is computed to be 7 dB, while its average value at frequencies higher than 9.4 Hz is 3 dB. Fig. 24 shows the corresponding response of the equipment velocity per base velocity.

In sum, although force feedback control is a very effective control strategy, in real systems it raises robustness issues, which greatly limit its performance. Also, if the aim of the controller is to minimize the equipment velocity, force feedback is not a good solution.

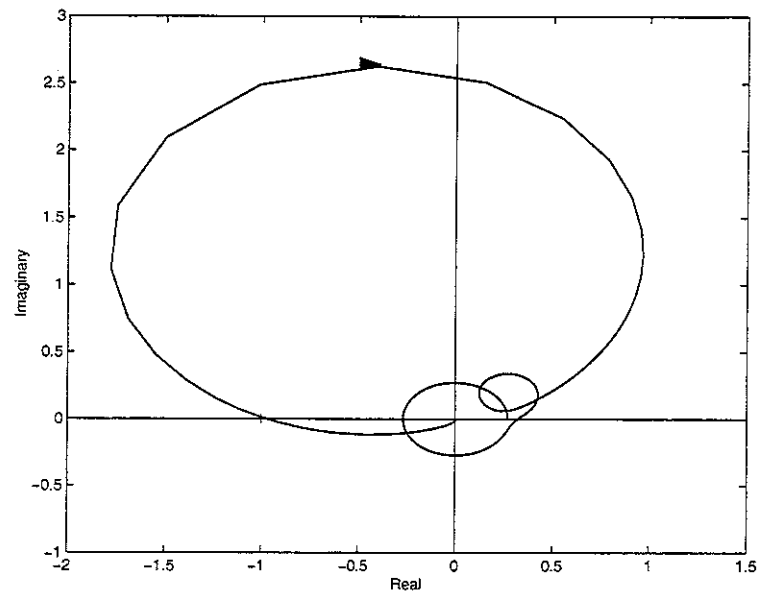

Fig. 22 *Nyquist plot of the transfer function between secondary excitation and total force of a realistic vibration isolation system with an inertial actuator and force feedback control. Realistic electronic components are used, the time delay is assumed to be 0.01 seconds, and the feedback gain is set to 0.036. ω varies from 0 to $+\infty$.*

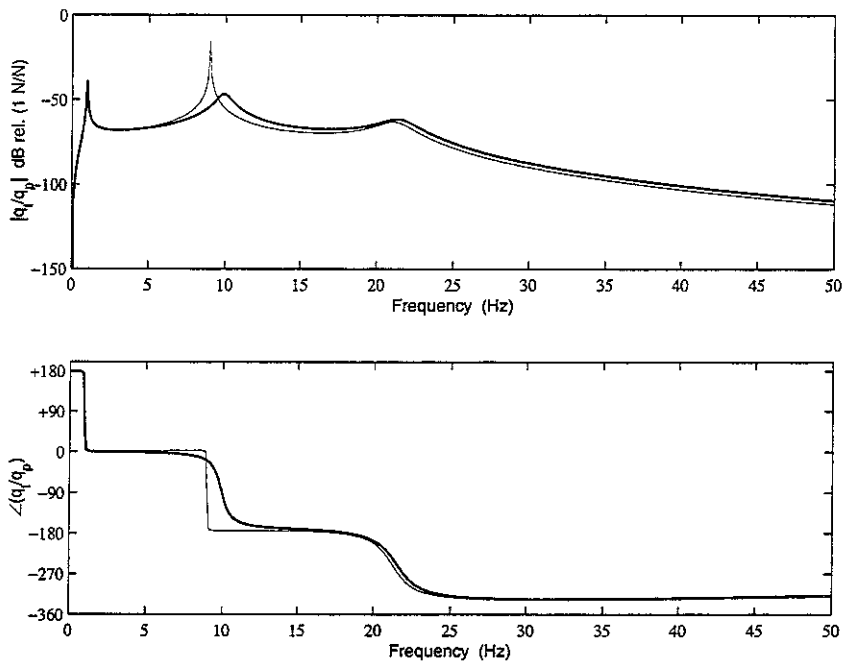

Fig. 23 *Bode plot of the transfer function between primary excitation and total force of the ideal system without control (solid line) and the realistic (faint line) vibration isolation system with an inertial actuator and force feedback control. Realistic electronic components are used, the time delay is assumed to be 0.001 seconds, and the feedback gain is set to 0.036.*

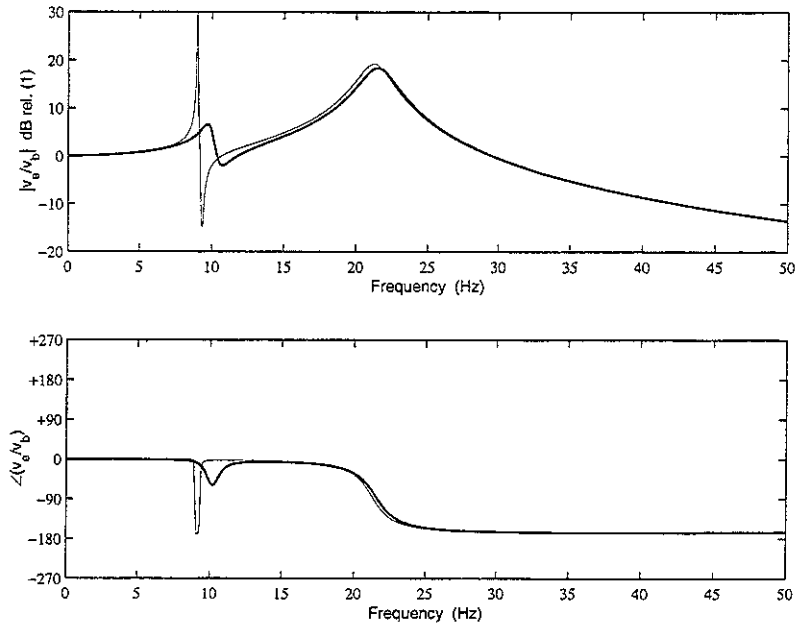

Fig. 24 *Transmissibility of the ideal system without control (solid line) and the realistic (faint line) vibration isolation system with an inertial actuator and force feedback control. Realistic electronic components are used, the time delay is assumed to be 0.001 seconds, and the feedback gain is set to 0.036.*

2.4 Integrated Force Feedback Control

By replacing the force gain in Fig. 15 with an integrator, an integrated force feedback controller is obtained. The total force is measured, integrated, and then fed back into the inertial actuator. Analytically, the equation for the whole structure is given by (2.26), while the control law is described by

$$q_a = -h_{if} \frac{q_t}{j\omega} \tag{2.39}$$

The Bode plot (Fig. 25), the Nyquist plot (Fig. 26) and the root locus (Fig. 27) show a very interesting behaviour. The ideal system is unconditionally stable and in particular at low frequencies the system dynamics tends to increase its damping and its robustness.
It can be noted that the integrated force being fed back is proportional to the absolute velocity of the actuator mass.
Problems for real systems arise at high frequency, though. In the Nyquist plot, the second smaller loop, due to the passive mount interaction with the base end equipment, is very close to the x-axis. This property can be validated by analysing the root locus and in particular the behaviour of the high frequency complex conjugate poles. When the feedback gain h_{if} is increased, the mode tends to get very close to the imaginary axis. High frequency instabilities in the active feedback control system typically arise from four sources: low-pass filter module of the charge amplifier, control force shakers, accelerometers, and time delays. Due to any or a combination of these causes, the high frequency loop in the Nyquist plot may cross the x-axis, causing a closed loop instability

for a certain critical gain. Thus, in real systems with high frequency electronic flaws, the integrated force feedback control may be conditionally stable.

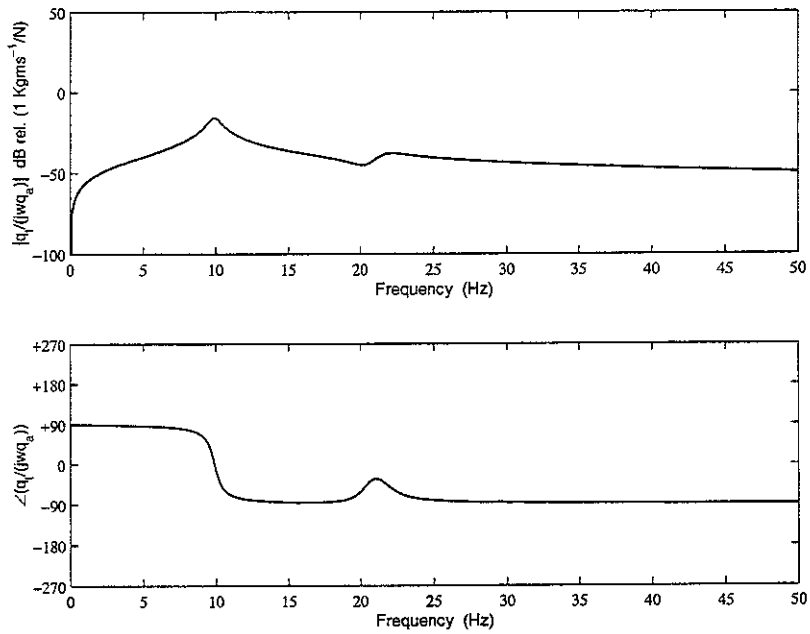

Fig. 25 *Bode plot of the integrated force per secondary excitation of a vibration isolation system with an inertial actuator and integrated force feedback control.*

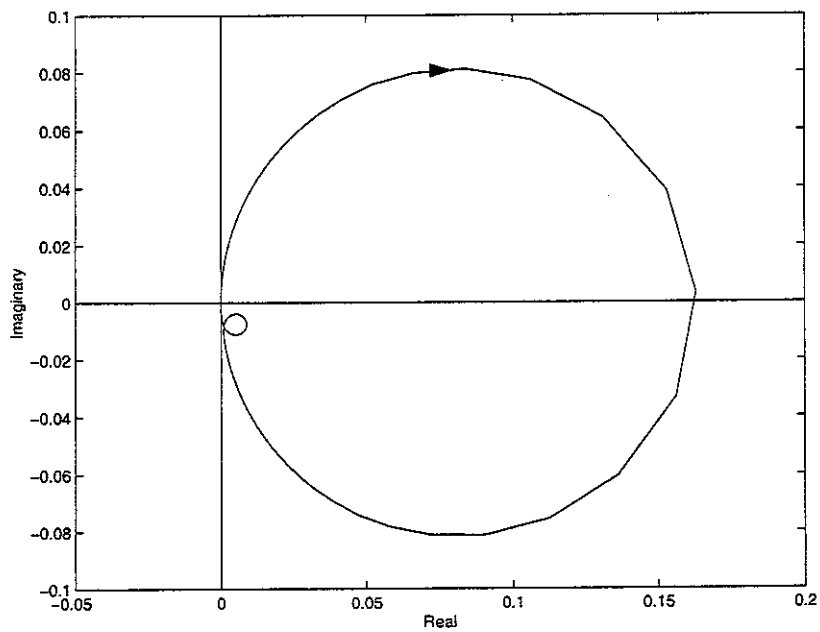

Fig. 26 *Nyquist plot of the transfer function between secondary excitation and integrated force of a vibration isolation system with an inertial actuator and integrated force feedback control. ω varies from 0 to $+\infty$.*

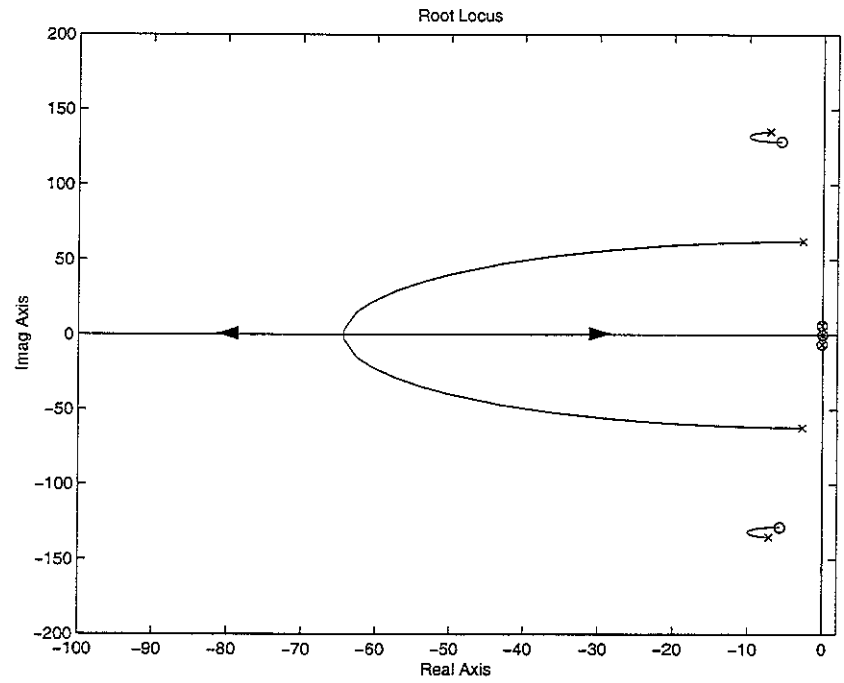

Fig. 27 *Root locus of the transfer function between secondary excitation and integrated force of a vibration isolation system with an inertial actuator and integrated force feedback control.*

The total force measured by the force transducer per primary excitation is reported in Fig. 28, and its equation is given by

$$q_t = \frac{j\omega Y_e Y_b Z_m B}{j\omega[1 + Z_m(Y_b + Y_e + Y_e B Y_b) + Y_e B] + A(1 + Z_m(Y_b + Y_e)h_{if}} q_p \quad (2.40)$$

Fig. 29 shows the equipment velocity response per base response, which is given by

$$\frac{v_e}{v_b} = \frac{j\omega Y_e Z_m (1 + A h_{if})}{j\omega[1 + Z_m Y_e + Y_e B] + A(1 + Z_m Y_e)h_{if}} \quad (2.41)$$

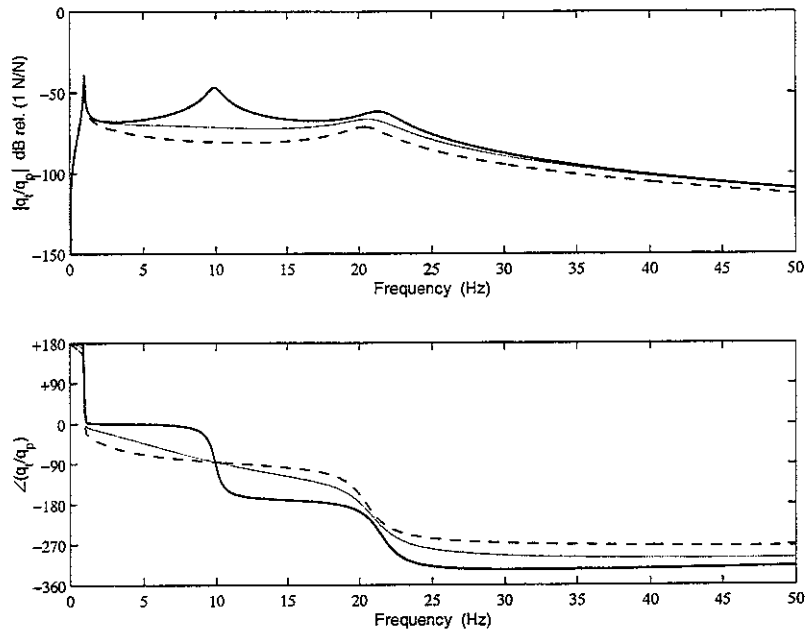

Fig. 28 *Bode plot of the transfer function between primary excitation and total force of a vibration isolation system based on an inertial actuator and integrated force feedback control. Three gains h_{fl} have been analysed: h_{if} = 0 (bold line), h_{if} = 100 (faint line), and h_{if} = 300 (dashed line.)*

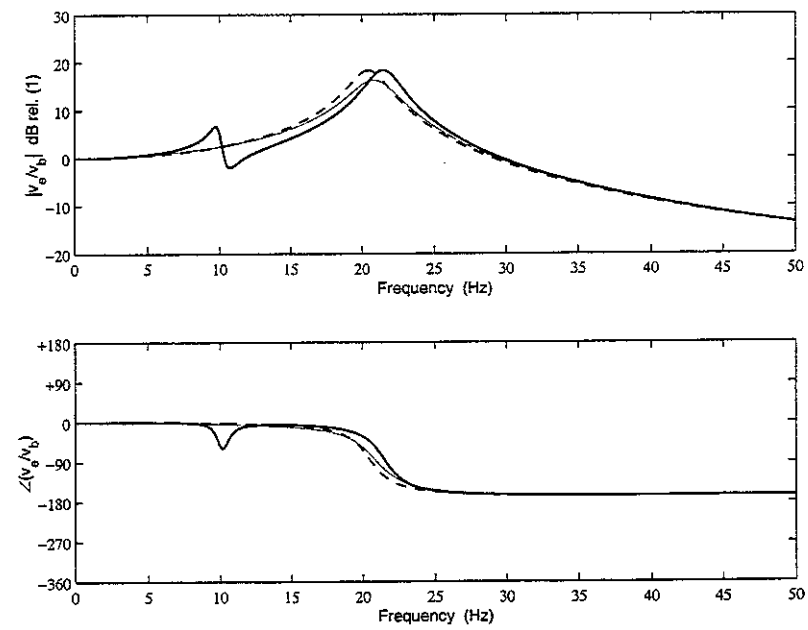

Fig. 29 *Transmissibility of a vibration isolation system with an inertial actuator and integrated force feedback control. Three gains h_{fl} have been analysed: h_{if} = 0 (bold line), h_{if} = 100 (faint line), and h_{if} = 300 (dashed line.)*

A robust analysis on the system with integrated force feedback is described by the equations (2.32), and from (2.34) to (2.39) illustrate the dynamics of the components. In particular:

$$H(j\omega) = \frac{-\omega^2 h_{if}\, 0.1326}{(1+ j\omega 0.1326)^2} \cdot \frac{1}{1+ j\omega 0.251} \tag{2.41}$$

Given the realistic system described above, and also assuming a time delay T=0.001 seconds, the maximum gain h_{if} that guarantees the system to be stable is 8.5. This is illustrated in Fig. 30. For this value of the gain, the maximum attenuation in the closed loop response (Fig. 31) is computed to be 33 dB, while the average is 8 dB within a very large frequency range between 5.2 Hz, where the Nyquist point is passed, and at least 2 kHz, upper bound of the computer simulation. This method is not only robust, but performance is also very acceptable, if compared to the other solutions described so far.
Fig 32 shows the transmissibility of the system. In sum, integrated force control is a good choice in terms of reducing the transmitted force, while it is a poor strategy if the aim is equipment velocity attenuation.

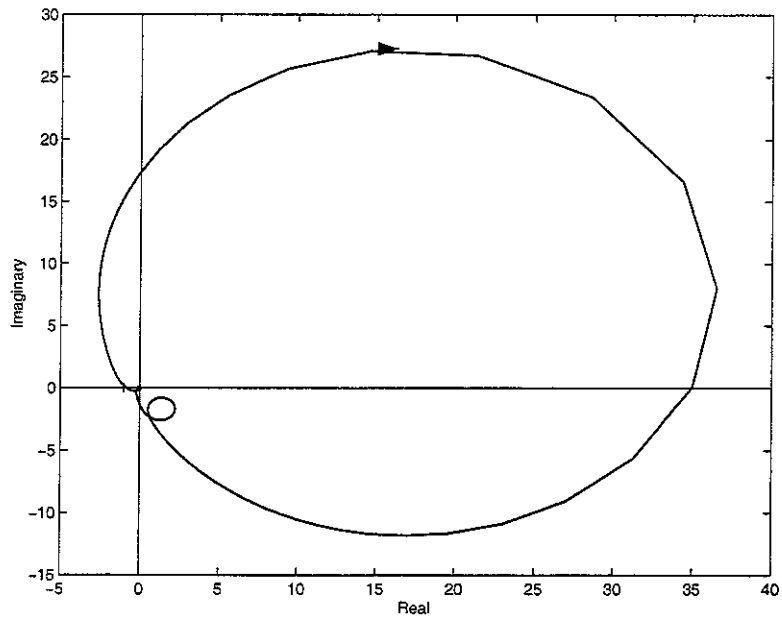

Fig. 30 *Nyquist plot of the transfer function between secondary excitation and integrated total force of a realistic vibration isolation system with an inertial actuator and integrated force feedback control. Realistic electronic components are used, the time delay is assumed to be 0.001 seconds, and the feedback gain is 8.5. ω varies from 0 to $+\infty$.*

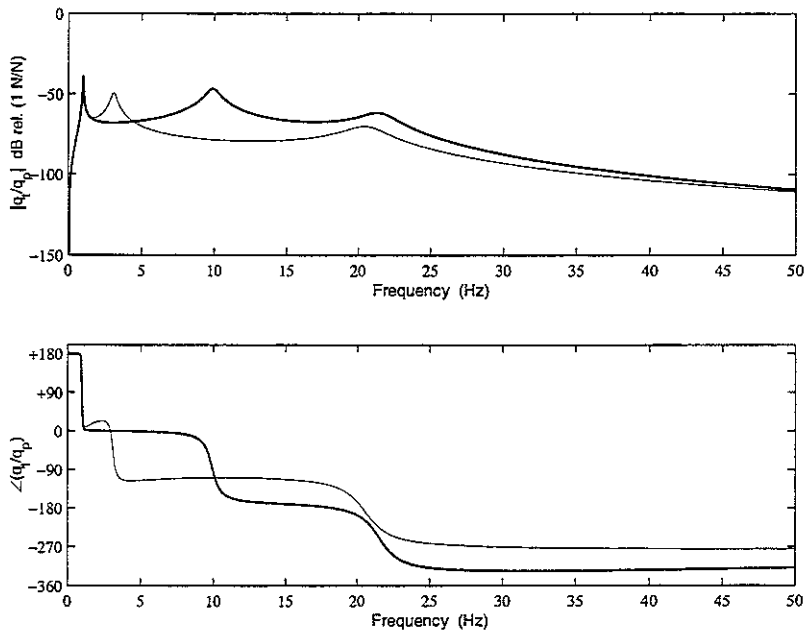

Fig. 31 *Bode plot of the transfer function between primary excitation and total force of the ideal system without control (solid line) and the realistic (faint line) vibration isolation system with an inertial actuator and integrated force feedback control. Realistic electronic components are used, the time delay is assumed to be 0.001, and the feedback gain is set to 8.5.*

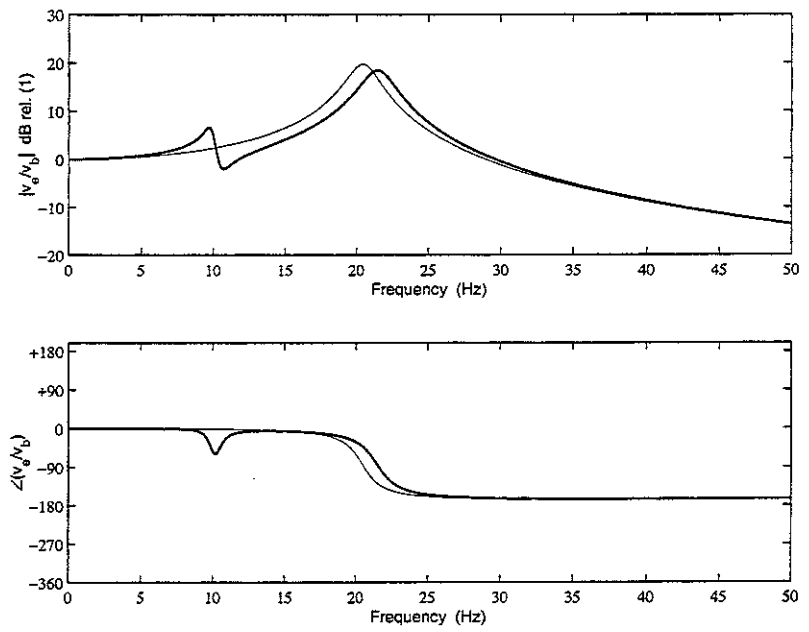

Fig. 32 *Transmissibility of the ideal system without control (solid line) and the realistic (faint line) vibration isolation system with an inertial actuator and integrated force feedback control. Realistic electronic components are used, the time delay is assumed to be 0.001, and the feedback gain is set to 8.5.*

2.5 Force and Velocity Feedback Control

A combination of force and velocity feedback control is now studied. The control to the inertial actuator is the sum of a total force feedback and a velocity feedback, therefore two sensors are needed (force and velocity) and one actuator. This transforms the control problem into a multiple-input-single-output (MISO) system. The aim of this and the following sections is to find an appropriate set of gains for different control loop strategies in order to minimize the equipment velocity. The block diagram of a multichannel feedback control system is shown in Fig. 33.

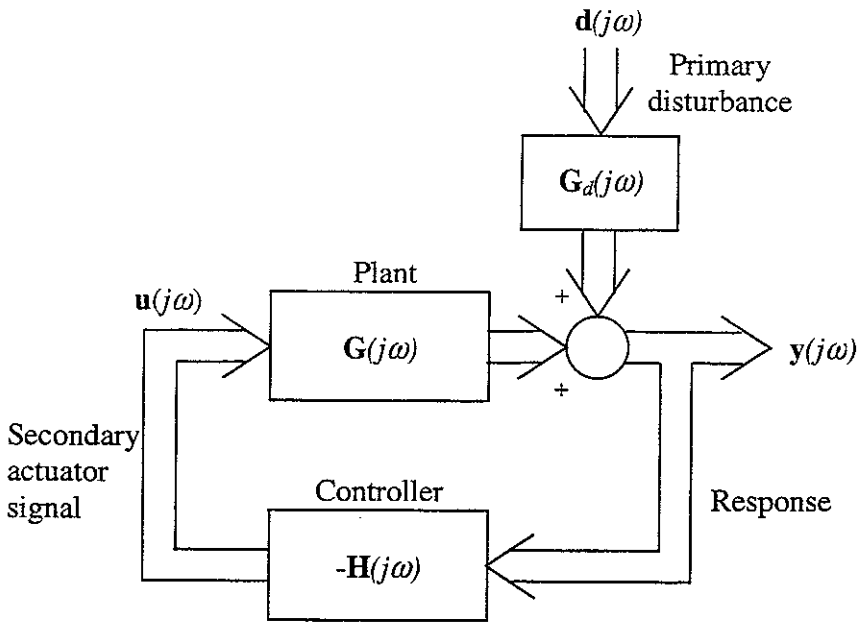

Fig. 33 *Block diagram of a multichannel feedback control system including the plant, the controller, and the disturbance source.*

From the block diagram follows that

$$\mathbf{y}(j\omega) = \frac{\mathbf{G}_d(j\omega)}{I + \mathbf{G}(j\omega)\mathbf{H}(j\omega)}\mathbf{d}(j\omega) \tag{2.42}$$

The application of the force and velocity controller to the system is presented in Fig. 34. In this case, both total force and velocity are measured at the equipment. While (2.42) still holds, the output and input variables are

$$\mathbf{y}(j\omega) = \begin{Bmatrix} v_e \\ q_t \end{Bmatrix} \tag{2.43}$$

$$\mathbf{d}(j\omega) = \{q_p\} \tag{2.44}$$

$$\mathbf{u}(j\omega) = \{q_a\} \tag{2.45}$$

The system equation is given by

$$\begin{Bmatrix} v_e \\ q_t \end{Bmatrix} = \mathbf{G}(j\omega)\{q_a\} + \mathbf{G}_d(j\omega)\{q_p\} \tag{2.46}$$

and the control law can be written as

$$\{q_a\} = -\mathbf{H}(j\omega)\begin{Bmatrix} v_e \\ q_t \end{Bmatrix} \tag{2.47}$$

where

$$\mathbf{G}(j\omega) = \begin{bmatrix} \dfrac{Y_e A(1+Y_b Z_m)}{1+Z_m(Y_e+Y_b+Y_e B Y_b)+Y_e B} \\ \dfrac{A(1+Z_m(Y_e+Y_b))}{1+Z_m(Y_e+Y_b+Y_e B Y_b)+Y_e B} \end{bmatrix} \tag{2.48}$$

$$\mathbf{G}_d(j\omega) = \begin{bmatrix} \dfrac{Y_e Y_b Z_m}{1+Z_m(Y_e+Y_b+Y_e B Y_b)+Y_e B} \\ \dfrac{B Y_e Y_b Z_m}{1+Z_m(Y_e+Y_b+Y_e B Y_b)+Y_e B} \end{bmatrix} \tag{2.49}$$

$$\mathbf{H}(j\omega) = \begin{bmatrix} h & h_f \end{bmatrix} \tag{2.50}$$

In terms of transmissibility, the above equations can be rewritten as

$$\mathbf{y}(j\omega) = \begin{Bmatrix} v_e \\ q_t \end{Bmatrix} \tag{2.51}$$

$$\mathbf{d}(j\omega) = \{v_b\} \tag{2.52}$$

$$\mathbf{u}(j\omega) = \{q_a\} \tag{2.53}$$

$$\begin{Bmatrix} v_e \\ q_t \end{Bmatrix} = \mathbf{G}(j\omega)\{q_a\} + \mathbf{G}_d(j\omega)\{v_b\} \tag{2.54}$$

$$\{q_a\} = -\mathbf{H}(j\omega)\begin{Bmatrix} v_e \\ q_t \end{Bmatrix} \tag{2.55}$$

$$\mathbf{G}(j\omega)=\begin{bmatrix}\dfrac{Y_eA}{1+Z_mY_e+Y_eB}\\ \dfrac{A(1+Z_mY_b)}{1+Z_mY_e+Y_eB}\end{bmatrix} \tag{2.56}$$

$$\mathbf{G}_d(j\omega)=\begin{bmatrix}\dfrac{Y_eZ_m}{1+Z_mY_e+Y_eB}\\ \dfrac{BY_eZ_m}{1+Z_mY_e+Y_eB}\end{bmatrix} \tag{2.57}$$

$$\mathbf{H}(j\omega)=\begin{bmatrix}h & h_f\end{bmatrix} \tag{2.58}$$

while (2.42) still holds. Fig. 35 shows an equivalent schematic of a vibration isolation system. The equations describing the inner loop can be written as

$$q_t = Z_{open}v_e + Gq_a \tag{2.59}$$

$$q_a = H(f_c - q_t) \tag{2.60}$$

and substituting (2.60) into (2.59), the total measured force becomes

$$q_t = \frac{Z_{open}}{1+GH}v_e + \frac{GH}{1+GH}f_c \tag{2.61}$$

It should be noted that $Z_{closed} = \dfrac{Z_{open}}{1+GH} << Z_{open}$ and if $GH >> 1$ then $q_t \cong f_c$, which means that the total transmitted force can be regulated using the command signal, which is chosen to be the output of the outer control loop. The outer loop is a velocity feedback controller, and by doing so $\dfrac{q_t}{v_e} \cong Z_d$, which indicates that a skyhook damper is implemented.

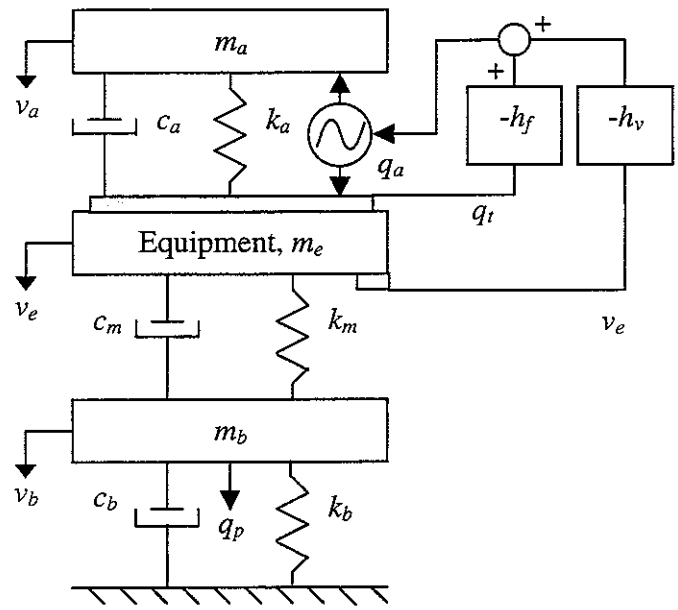

Fig. 34 *Schematic of a vibration isolation system with an inertial actuator and the sum of force and velocity feedback control.*

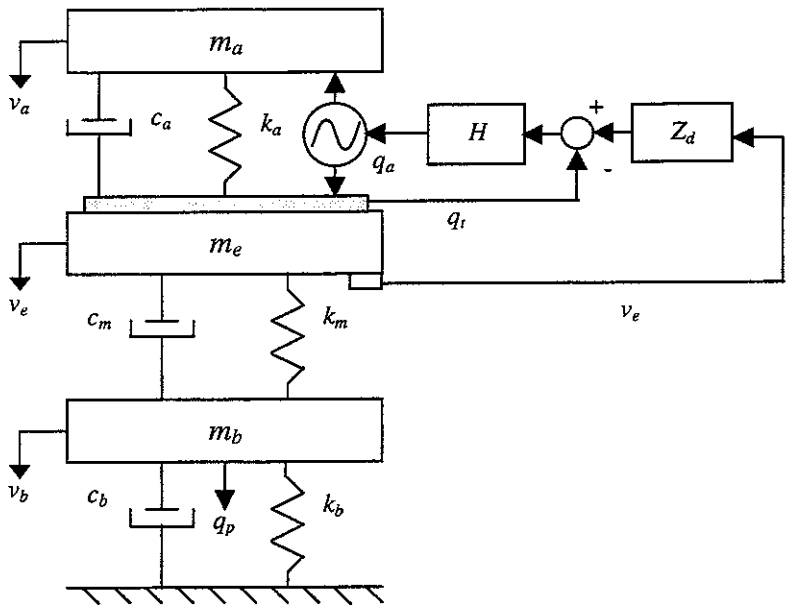

Fig. 35 *Equivalent schematic of a vibration isolation system with an inertial actuator and the sum of force and velocity feedback control.*

When the force control gain is set to zero and the velocity feedback gain can vary, the overall system behaves like the a DVFB system. In this case, there exist a velocity gain at which the curve passes through the origin, making the closed loop system unstable. At higher gain values, the curve encircles the critical point obtaining the same instability

effect. This behaviour was actually expected, since the system with velocity feedback and no force feedback is equivalent to the system of Fig. 2. Similarly, when the velocity feedback gain is set to zero and the force feedback gain can vary, the overall behaviour is equivalent to a force feedback control system.

A very interesting behaviour is found when the two controllers are operative simultaneously, as illustrated by the Nyquist plot in Fig. 34. Starting from a stable initial system, when the velocity gain is increased above the critical point, the closed loop system becomes unstable (faint line.) At this point, if the force control feedback gain is increased (dotted line), the overall ideal closed loop system becomes unconditionally stable again. In sum, it is found that force feedback control is able to stabilize those systems with velocity feedback that are unstable due to the high velocity gain. Like in the previous case, the force controller adds an "apparent" mass to the inertial actuator mass, while the velocity controller adds damping to the system. An important aspect is that for a given force feedback control gain, the velocity feedback control gain that provides the same damping as the velocity gain used for a lower value of the force gain is greater. Alternatively, higher velocity gains are required in order to obtain the same damping effects when the force gain is increased.

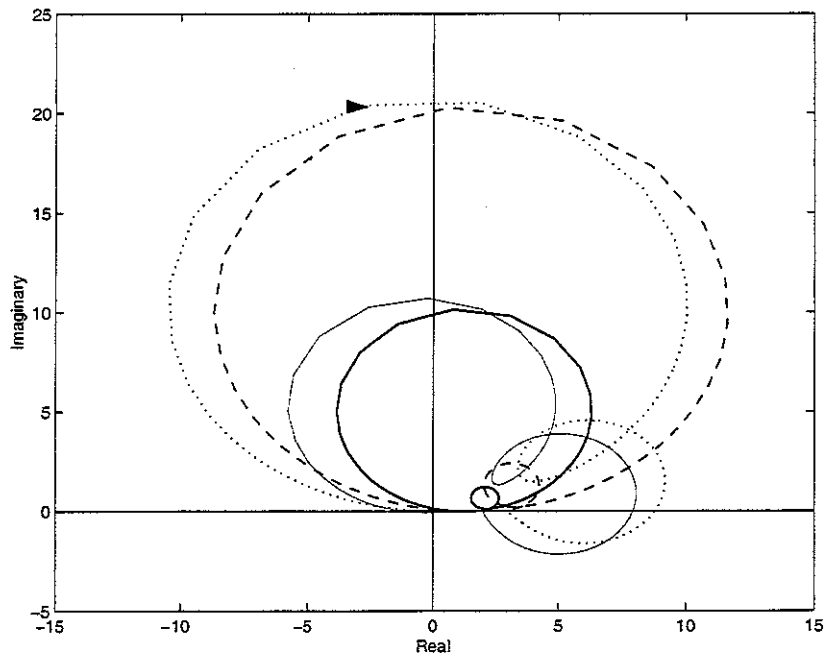

Fig. 36 *Multichannel Nyquist plot of the determinant of* $(\boldsymbol{I}+\boldsymbol{G}(j\omega)\boldsymbol{H}(j\omega))$. *The plant is a vibration isolation system with an inertial actuator. The controller is the sum of force and velocity feedback. In this case both force and velocity feedback effects are present:* $h_v = h_f = 1$ *(bold line),* $h_v = 200$ *and* $h_f = 1$ *(faint line),* $h_v = 1$ *and* $h_f = 2$ *(dashed line),* $h_v = 200$ *and* $h_f = 2$ *(dotted line.)* ω *varies from 0 to* $+\infty$.

The question that must be posed now regards the performance of the double controller in the context of the complete system. Fig. 37 shows the effect of the primary excitation on the total measured force at the equipment. When force feedback control is added to the system, significant attenuation is experienced starting from the inertial actuator modal

frequency. Also, force feedback is able to stabilize systems (dotted line) that were unstable (faint line) by using velocity feedback only. Considering the total transmitted force to the equipment as the variable that must be minimized in order to have good vibration isolation of the equipment, the conclusion is that force control is definitely a better solution than velocity control or even a combination of the two control strategies.
Fig. 38 shows the transmissibility of the system. Although the force feedback control does not seem to be very effective in adding damping to the system (the attenuation is not outstanding), it stabilizes the system (dotted line) that was previously unstable (faint line.) On the other hand, considering the equipment velocity as the variable that must be minimized for vibration isolation purposes, the velocity control strategy offers better results than the force controller, especially within the frequency range where the structural mode lies. However, force control is needed to stabilize unstable velocity controlled systems.

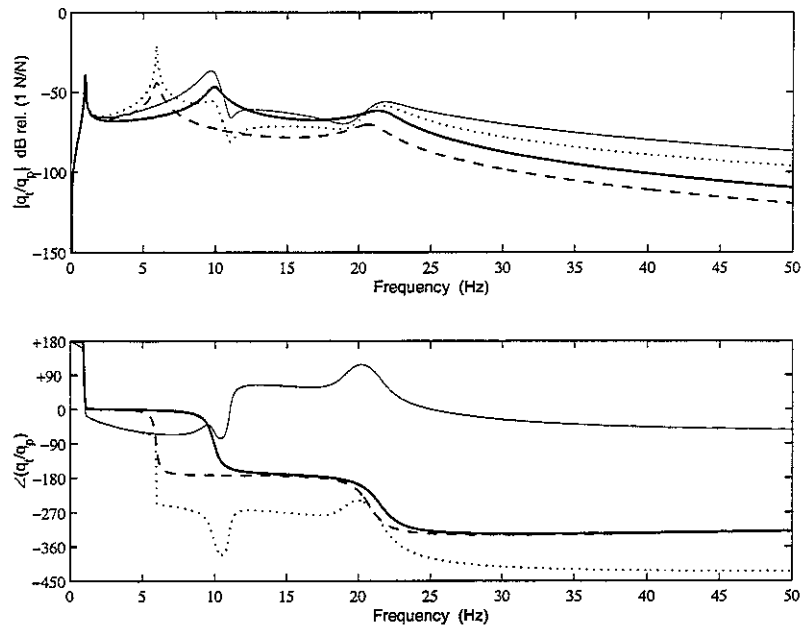

Fig. 37 *Bode plot of the transfer function between primary excitation and total measured force of a vibration isolation system with an inertial actuator and the sum of force and velocity feedback control. Four cases are reported:* $h_f = 0$ *and* $h_v = 0$ *(bold line),* $h_f = 0$ *and* $h_v = 200$ *(faint line, unstable),* $h_f = 2$ *and* $h_v = 0$ *(dashed line),* $h_f = 2$ *and* $h_v = 200$ *(dotted line.) The second case causes closed loop instability. This problem is solved by increasing the force gain.*

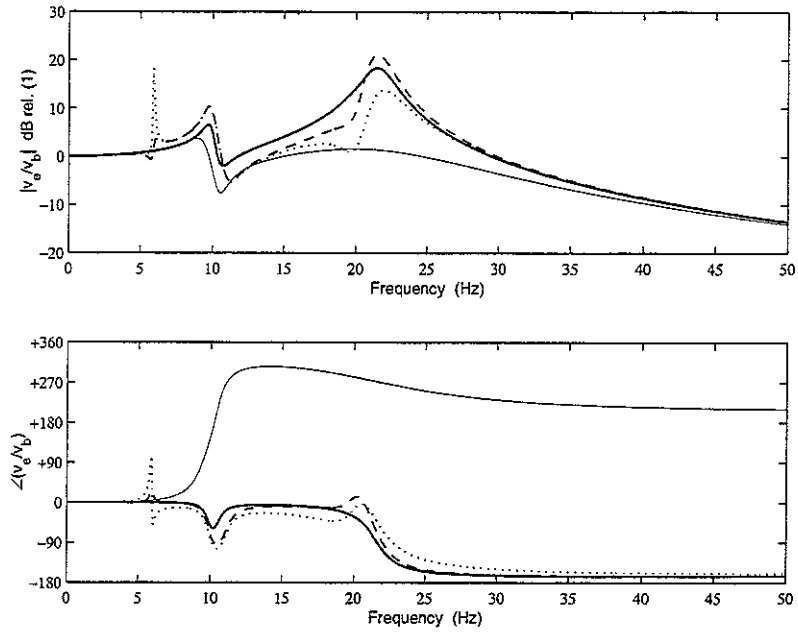

Fig. 38 *Transmissibility of a vibration isolation system based on an inertial actuator and the sum of force and velocity feedback control. Four cases are reported: $h_f = 0$ and $h_v = 0$ (bold line), $h_f = 0$ and $h_v = 200$ (faint line, unstable), $h_f = 2$ and $h_v = 0$ (dashed line), $h_f = 2$ and $h_v = 200$ (dotted line.) If $h_f = 0$ and $h_v = 200$ the system is unstable, but can be stabilized by increasing h_f to 2.*

A robust analysis on the system with force and velocity feedback is now proposed. Fig. 39 shows a realistic block diagram for the real system.

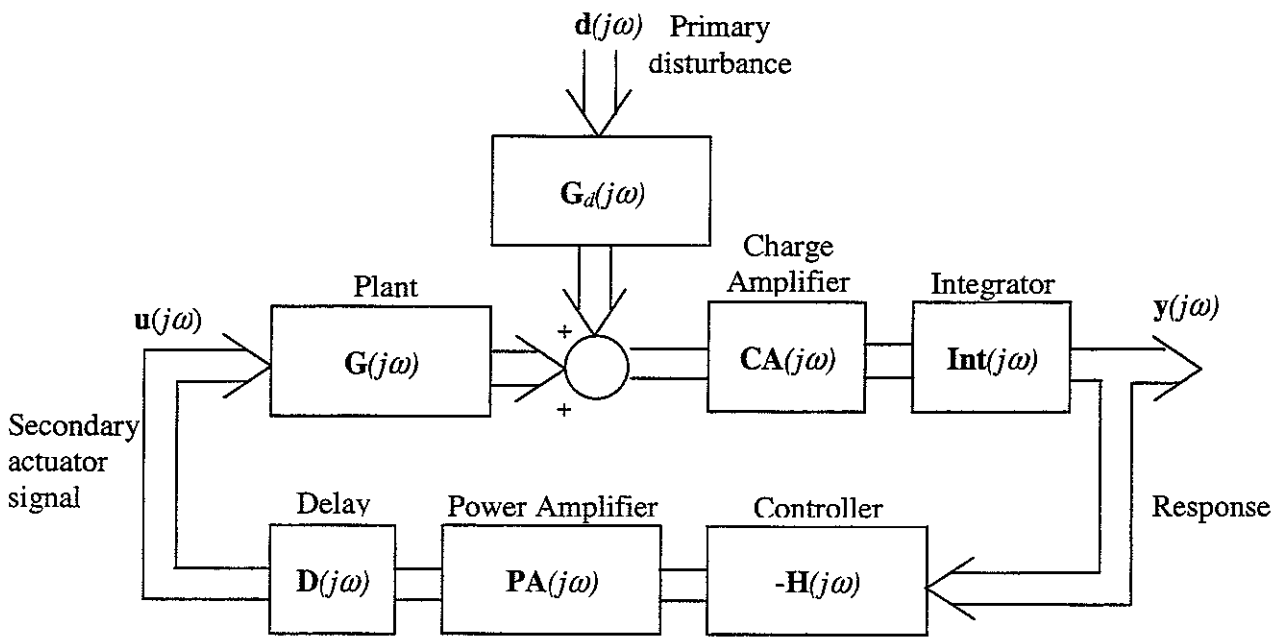

Fig. 39 *Block diagram of a real negative feedback control system including the plant, the integrated force controller, and the electronic components.*

The following equations illustrate the dynamics of the components in Fig. 39. The numerical values have been chosen according to off-the-shelf commercial components. Like in the previous analysis, the charge amplifier cut-off frequency is 1 Hz and each controller is modelled using a second order high pass filter, simulating the gain electronics:

$$\mathbf{G}(j\omega) = \begin{bmatrix} \dfrac{j\omega Y_e A(1+Y_b Z_m)}{1+Z_m(Y_e+Y_b+Y_e B Y_b)+Y_e B} \\ \dfrac{A(1+Z_m(Y_e+Y_b))}{1+Z_m(Y_e+Y_b+Y_e B Y_b)+Y_e B} \end{bmatrix} \tag{2.62}$$

$$\mathbf{H}(j\omega) = \begin{bmatrix} \dfrac{-\omega^2 h 0.1326}{(1+j\omega 0.1326)^2} & \dfrac{-\omega^2 h_f 0.1326}{(1+j\omega 0.1326)^2} \end{bmatrix} \tag{2.63}$$

$$\mathbf{CA}(j\omega) = \begin{bmatrix} \dfrac{j\omega 0.159}{1+j\omega 0.159} \\ \dfrac{j\omega 0.2385}{1+j\omega 0.2385} \end{bmatrix} \tag{2.64}$$

$$\mathbf{Int}(j\omega) = \begin{bmatrix} \dfrac{1}{1+j\omega 0.251} \\ 1 \end{bmatrix} \tag{2.65}$$

$$\mathbf{PA}(j\omega) = \begin{bmatrix} \dfrac{j\omega 0.1326}{1+j\omega 0.1326} & \dfrac{j\omega 0.1326}{1+j\omega 0.1326} \end{bmatrix} \tag{2.66}$$

$$\mathbf{D}(j\omega) = \begin{bmatrix} e^{-j\omega 0.001} & e^{-j\omega 0.001} \end{bmatrix} \tag{2.67}$$

The stability of this realistic multichannel control system is determined by examining whether the locus of the determinant of $[\mathbf{I}+\mathbf{G}_t(j\omega)\mathbf{H}_t(j\omega)]$ encloses the origin as ω varies from $-\infty$ to $+\infty$, where

$$\mathbf{G}_t(j\omega) = \mathbf{G}(j\omega) \tag{2.68}$$

$$\mathbf{H}_t(j\omega) = \mathbf{CA}(j\omega)\mathbf{Int}(j\omega)\mathbf{H}(j\omega)\mathbf{PA}(j\omega)\mathbf{D}(j\omega) \tag{2.69}$$

Only in (2.68) and (2.69) the product is an array multiplication, not a matrix multiplication. The closed loop frequency response function is given by

$$v_e = [\mathbf{I}+\mathbf{G}_t(j\omega)\mathbf{H}_t(j\omega)]^{-1}\mathbf{G}_d(j\omega)q_p \tag{2.70}$$

where

$$\mathbf{G}_d(j\omega) = \begin{bmatrix} \dfrac{j\omega Y_e Y_b Z_m}{1+Z_m(Y_e+Y_b+Y_e B Y_b)+Y_e B} \\ \dfrac{B Y_e Y_b Z_m}{1+Z_m(Y_e+Y_b+Y_e B Y_b)+Y_e B} \end{bmatrix} \tag{2.71}$$

A performance comparison follows. Given the realistic system in Fig. 39, described by (2.62) through (2.71), and also assuming a time delay T=0.001 seconds, a set of maximum gains h_i and h_f that guarantee the system to be stable are, respectively, 1.65 and 0.01. This is illustrated in Fig. 40. For these values of the gain, the maximum attenuation in the transmissibility (Fig. 42) is 8 dB, while its average is 4 dB within the 18-25 Hz frequency range. Regarding the attenuation of the force transmitted to the equipment (Fig. 41), this choice of feedback gains does not provide good results. In fact, rather than an attenuation, an amplification is experienced at frequencies greater than 20 Hz. It is important to notice that when h_i is dominant compared to h_f, the Nyquist plot assumes a shape that reminds of the DVFB case, while when h_f is dominant compared to h_i, the Nyquist plot reminds of the force feedback case. In the former case, the equipment velocity performance is privileged with respect to the total transmitted force, whereas in the latter case the opposite occurs. In sum, the two gains act like two tuneable devices: h_i improves the equipment velocity attenuation, h_f is more effective on the total transmitted force attenuation. In other words, it is a matter of balancing the two values within the stability region, which does not mean that setting the two gains to their maximum values, which were obtained in both the DVFB and force feedback cases, guarantees the best performance of the MIMO system. In general this solution leads to an unstable system.

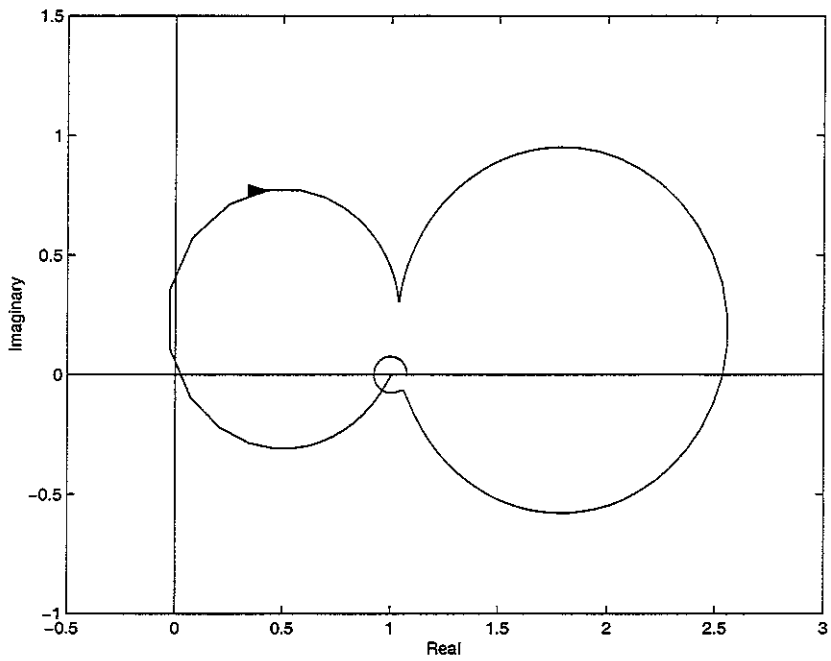

Fig. 40 *Multichannel Nyquist plot of the determinant of* $(\boldsymbol{I}+\boldsymbol{G}(j\omega)\boldsymbol{H}(j\omega))$. *The plant is a realistic vibration isolation system with an inertial actuator. The controller is the sum of force and velocity feedback. Realistic electronic components are used, the time delay is assumed to be 0.001 seconds, the force feedback gain is 0.01, and the velocity feedback gain is 1.65.* ω *varies from 0 to* $+\infty$.

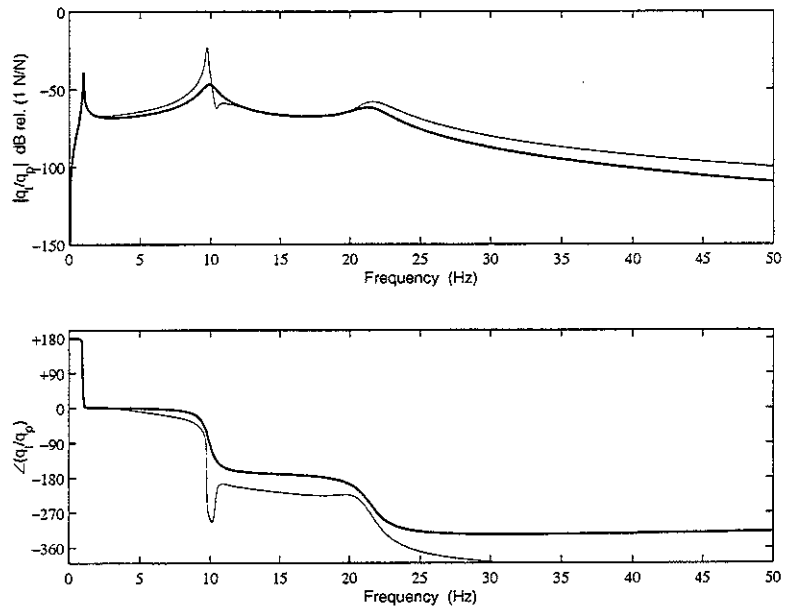

Fig. 41 *Bode plot of the transfer function between primary excitation and total measured force of the ideal system without control (solid line) and the realistic (faint line) vibration isolation system with the sum of force and velocity feedback control. Realistic electronic components are used, the time delay is assumed to be 0.001 seconds, the force feedback gain is set to 0.01, and the velocity feedback gain is set to 1.65.*

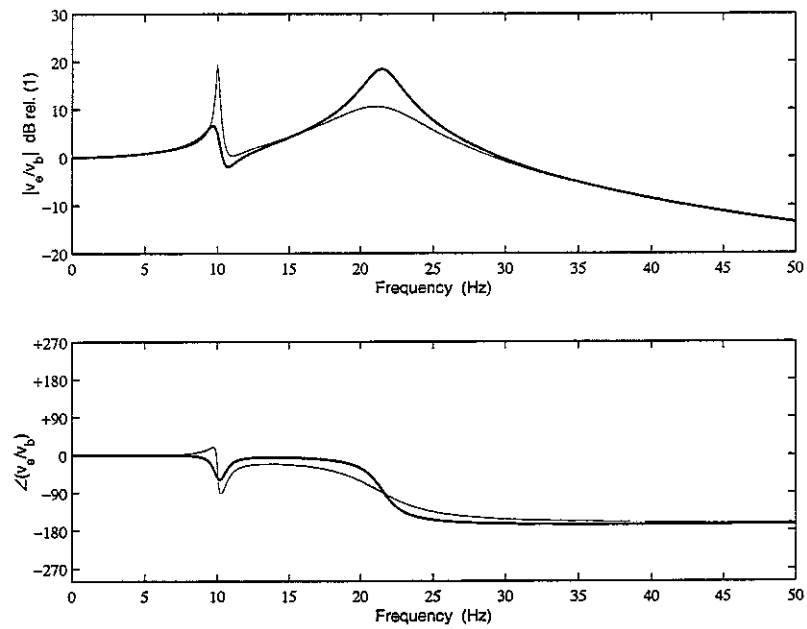

Fig. 42 *Transmissibility of the ideal system without control (solid line) and the realistic (faint line) vibration isolation system with the sum of force and velocity feedback control. Realistic electronic components are used, the time delay is assumed to be 0.001 seconds, the force feedback gain is set to 0.01, and the velocity feedback gain is set to 1.65.*

A combination of force and integrated velocity was also analysed, but the results are quite similar to the previous case both in terms of robustness and performance. 6 dB was the maximum attenuation and about 4 dB was the average (within a limited bandwidth) of the equipment velocity closed loop response. With respect to the previous case, the only advantage is that there is attenuation in the transmitted force for most of the selected control gains. This solution does not offer more than a mere integrated velocity feedback.

2.6 Integrated Force and Velocity Feedback

Among the energy absorbing controls, DVFB and integrated force feedback control are two of the most effective treatments. When these methods are both applied to the system in Fig. 1, the obtained Nyquist plot is shown in Fig. 43. Equations (2.42) through (2.49) describe the ideal system, with the exception of the control law, which in this case is given by

$$\mathbf{H}(j\omega) = \begin{bmatrix} h_v & \dfrac{h_{if}}{j\omega} \end{bmatrix} \tag{2.72}$$

The ideal closed loop system is conditionally stable when the velocity gain dominates over the integrated force gain, whereas when either the integrated force gain dominates or when the two gains are balanced, the closed loop system is unconditionally stable. This is not true for real systems, as expected.

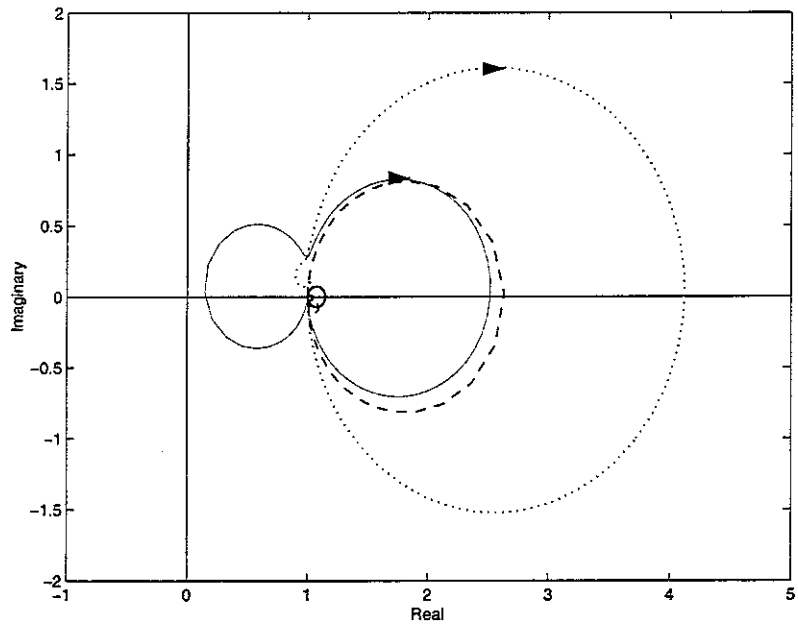

Fig. 43 *Multichannel Nyquist plot of the determinant of* $(\mathbf{I}+\mathbf{G}(j\omega)\mathbf{H}(j\omega))$. *The plant is a vibration isolation system with an inertial actuator. The controller is the sum of integrated force and velocity feedback. Different force feedback and velocity feedback gains are reported:* $h_{if} = 1$ *and* $h_v = 1$ *(bold line),* $h_{if} = 0$ *and* $h_v = 50$ *(faint line),* $h_{if} = 10$ *and* $h_v = 0$ *(dashed line),* $h_{if} = 10$ *and* $h_v = 100$ *(dotted line.)* ω *varies from 0 to* $+\infty$.

Fig. 44 shows the effect of the primary excitation on the total measured force, while Fig. 45 shows the transmissibility of the system. Performance greatly depends on the choice of the two feedback gains.

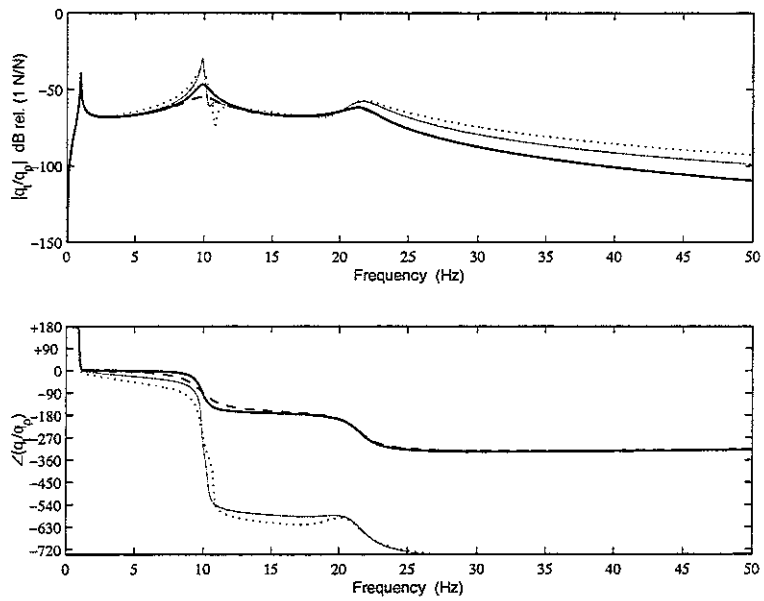

Fig. 44 *Bode plot of the transfer function between primary excitation and total force of a vibration isolation system with sum of integrated force and velocity feedback control. Different force feedback and velocity feedback gains are reported:* $h_{if} = 0$ *and* $h_v = 0$ *(bold line, no control),* $h_{if} = 0$ *and* $h_v = 50$ *(faint line),* $h_{if} = 10$ *and* $h_v = 0$ *(dashed line),* $h_{if} = 10$ *and* $h_v = 100$ *(dotted line.)*

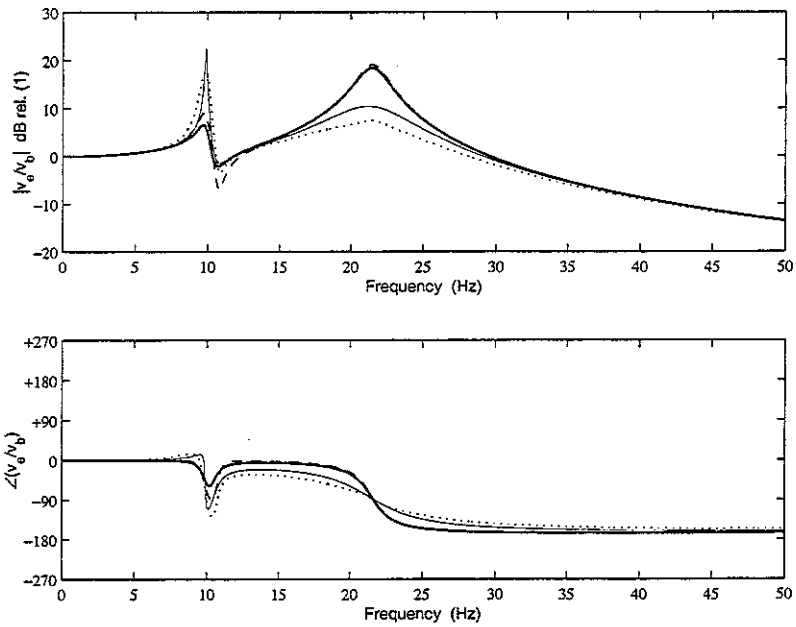

Fig. 45 *Transmissibility of a vibration isolation system with sum of integrated force and velocity feedback control. Different force feedback and velocity feedback gains are reported:* $h_{if} = 0$ *and* $h_v = 0$ *(bold line, no control),* $h_{if} = 0$ *and* $h_v = 50$ *(faint line),* $h_{if} = 10$ *and* $h_v = 0$ *(dashed line),* $h_{if} = 10$ *and* $h_v = 100$ *(dotted line.)*

For realistic systems based on integrated force and velocity feedback control, equations (2.62) through (2.71) describe the system, except for the control law, which is given by

$$\mathbf{H}(j\omega) = \left[\frac{-\omega^2 h 0.0633}{(1+j\omega 0.0633)^2} \quad \frac{-\omega^2 0.0633}{(1+j\omega 0.0633)^2} \cdot \frac{h_f}{1+j\omega 0.251} \right] \tag{2.73}$$

Such a high time constant for the integrator within the force feedback device implies that a very precise integrator is used. This time constant determines the size of the first internal low frequency loop: the smaller the time constant, the bigger the size of the loop.
Fig. 46 shows the Nyquist plot when a 0.001 second time delay is assumed, h_v = 50 and h_{if}=6, while Fig. 47 and Fig. 48 report the closed loop behaviour.
Although about the inertial actuator resonance frequency a considerable amplification is present, the closed loop system is extremely robust. Also, performance is very promising: the maximum attenuation in the equipment velocity is 22 dB, and the average is 9 dB. In particular, the frequency range where the attenuation is effective is very large: from 12.5 Hz to at least 2 kHz.

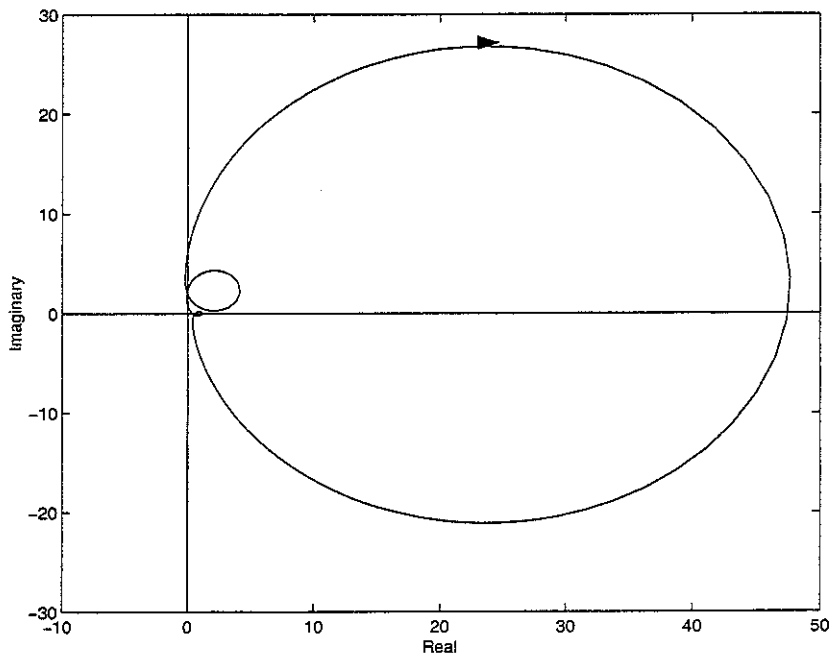

Fig. 46 *Multichannel Nyquist plot of the determinant of* $(\mathbf{I}+\mathbf{G}(j\omega)\mathbf{H}(j\omega))$. *The plant is a realistic vibration isolation system with an inertial actuator. The controller is the sum of integrated force and velocity feedback. Realistic electronic components are used, the time delay is assumed to be 0.001 seconds, the force feedback gain is 6, and the velocity feedback gain is 50.* ω *varies from 0 to* $+\infty$.

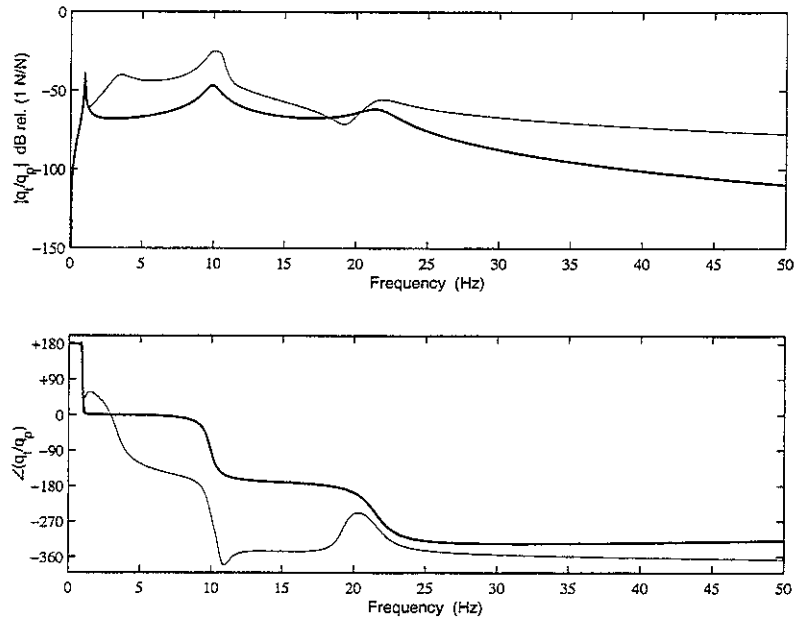

Fig. 47 *Bode plot of the transfer function between primary excitation and total force of the ideal system without control (solid line) and the realistic (faint line) vibration isolation system with an inertial actuator and the sum of integrated force and velocity feedback control. Realistic electronic components are used, the time delay is assumed to be 0.001 seconds, the force feedback gain is 6, and the velocity feedback gain is 50.*

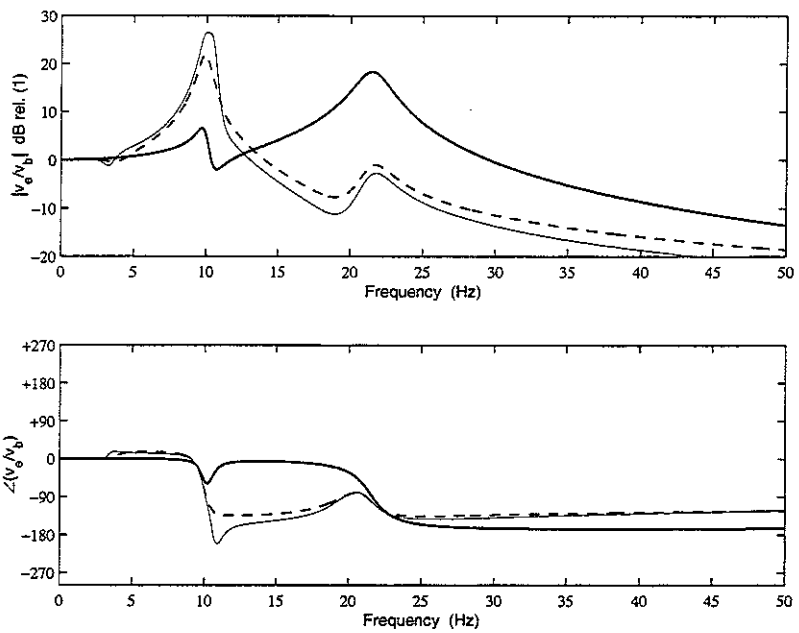

Fig. 48 *Transmissibility of ideal system without control (solid line) and the realistic (faint line) vibration isolation system with on an inertial actuator and the sum of force and velocity feedback control. Realistic electronic components are used, the time delay is set to 0.001 s, the force gain is 6 (faint) or 4 (dashed), and the velocity gain is 50 (faint) or 30 (dashed.)*

As Fig. 47 shows, the transmitted force to the equipment has increased, while the equipment velocity (Fig. 48) has decreased in a very wide frequency range. This is due to the choice of the control gains, which is aimed to minimize the equipment velocity. A different choice might be able to reduce the transmitted force. In other words, the double loop control structure allows the user to tune the system in order to achieve different control strategies. For example, if the choice of the feedback gains in Fig. 48 (faint line) is considered not appropriate because of the increased value of the transmissibility within the actuator resonance, another set of gains leads to a more robust system (dashed line.) In any case, even if the performance of this latter system is worse than the former, it remains far better than any other strategy studied in this work.

2.7 Integrated Force and Integrated Velocity Feedback

When SISO systems were analysed, in order to have the equipment velocity minimized, the integrated velocity feedback turned out to be a good solution with respect to performance and robustness. At the same time, in order to minimize the total transmitted force, the integrated force feedback method seems to be a very good approach. When these two methods are combined together in a MIMO system, the control law is given by

$$\mathbf{H}(j\omega) = \begin{bmatrix} \dfrac{h_{iv}}{j\omega} & \dfrac{h_{if}}{j\omega} \end{bmatrix} \tag{2.74}$$

The Nyquist plot is reported in Fig. 49. Even in this case, when h_{iv} is dominant, the behaviour of the system becomes integrated velocity feedback oriented, while integrated force feedback describes better the system when h_{if} is dominant. In any case, the ideal system is unconditionally stable. Also, the integrated force feedback tends to make the overall system more robust. On the other hand, the performance of this solution seems to be worse than the previous case. In fact, despite high gains are used, the equipment velocity behaviour does not improve significantly (Fig. 51.)

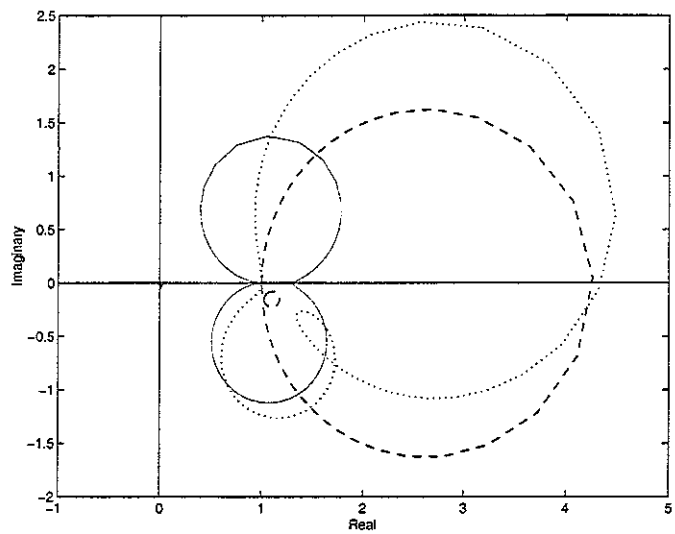

Fig. 49 *Multichannel Nyquist plot of the determinant of* $(I+G(j\omega)H(j\omega))$. *The controller is the sum of integrated force and integrated velocity feedback. Different force feedback and velocity feedback gains are reported:* $h_{if} = 1$ *and* $h_v = 1$ *(bold line),* $h_{if} = 0$ *and* $h_v = 5000$ *(faint line),* $h_{if} = 20$ *and* $h_v = 0$ *(dashed line),* $h_{if} = 20$ *and* $h_v = 5000$ *(dotted line.)* ω *varies from 0 to* $+\infty$.

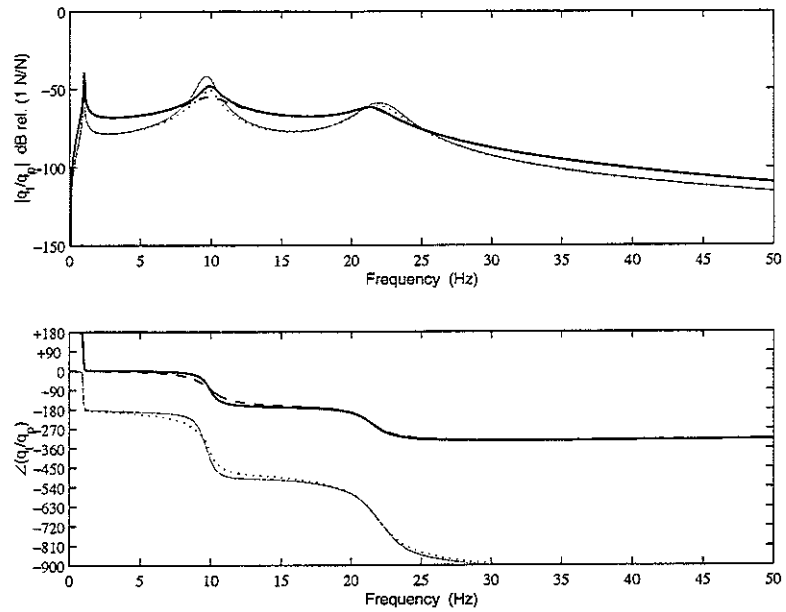

Fig. 50 *Bode plot of the transfer function between primary excitation and total force of a vibration isolation system with the sum of integrated force and integrated velocity feedback control. Different force feedback and velocity feedback gains are reported:* $h_{if} = 0$ *and* $h_v = 0$ *(bold line),* $h_{if} = 0$ *and* $h_v = 5000$ *(faint line),* $h_{if} = 20$ *and* $h_v = 0$ *(dashed line),* $h_{if} = 20$ *and* $h_v = 5000$ *(dotted line.)*

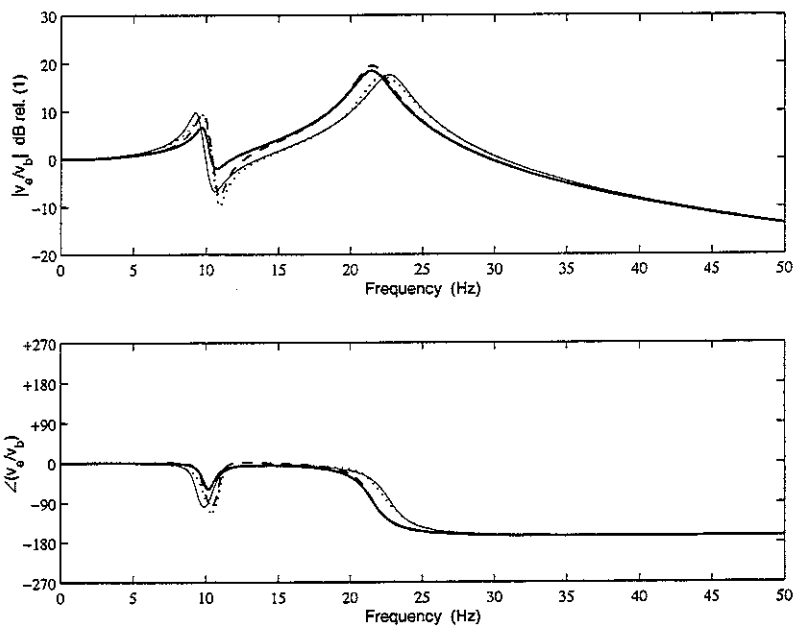

Fig. 51 *Transmissibility of a vibration isolation system with the sum of integrated force and integrated velocity feedback control. Different force feedback and velocity feedback gains are reported:* $h_{if} = 0$ *and* $h_v = 0$ *(bold line),* $h_{if} = 0$ *and* $h_v = 5000$ *(faint line),* $h_{if} = 20$ *and* $h_v = 0$ *(dashed line),* $h_{if} = 20$ *and* $h_v = 5000$ *(dotted line.)*

For a realistic system, (2.62) through (2.71) are assumed and the following describes the control law:

$$\mathbf{H}(j\omega) = \left[\frac{-\omega^2 0.0633}{(1+j\omega 0.0633)^2} \cdot \frac{h}{1+j\omega 0.0909} \quad \frac{-\omega^2 0.0633}{(1+j\omega 0.0633)^2} \cdot \frac{h_f}{1+j\omega 0.251} \right] \quad (2.75)$$

In this case Fig. 52 shows the relative Nyquist plot when h_{iv} =500 and h_{if}=2, and Fig. 53 and Fig. 54 report the closed loop performance compared to open loop case. Maximum effect was given to the ability of the velocity feedback to damp the equipment velocity response. In fact, the maximum attenuation for the total transmitted velocity is 20 dB, with an average value of 10 dB between the two main resonance frequencies.

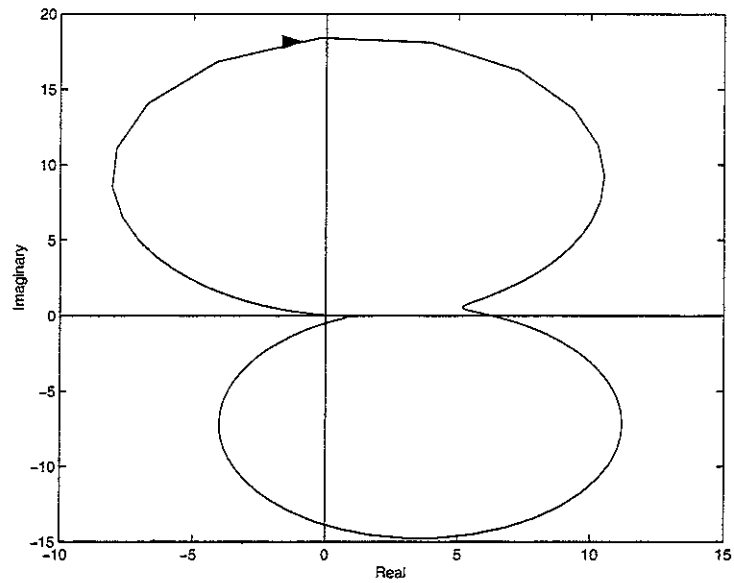

Fig. 52 *Multichannel Nyquist plot of the determinant of* $(\mathbf{I}+\mathbf{G}(j\omega)\mathbf{H}(j\omega))$. *The plant is a realistic vibration isolation system with an inertial actuator. The controller is the sum of integrated force and integrated velocity feedback. Realistic electronic components are used, the time delay is assumed to be 0.001 seconds, the force feedback gain is 2, and the velocity feedback gain is 500.* ω *varies from 0 to* $+\infty$.

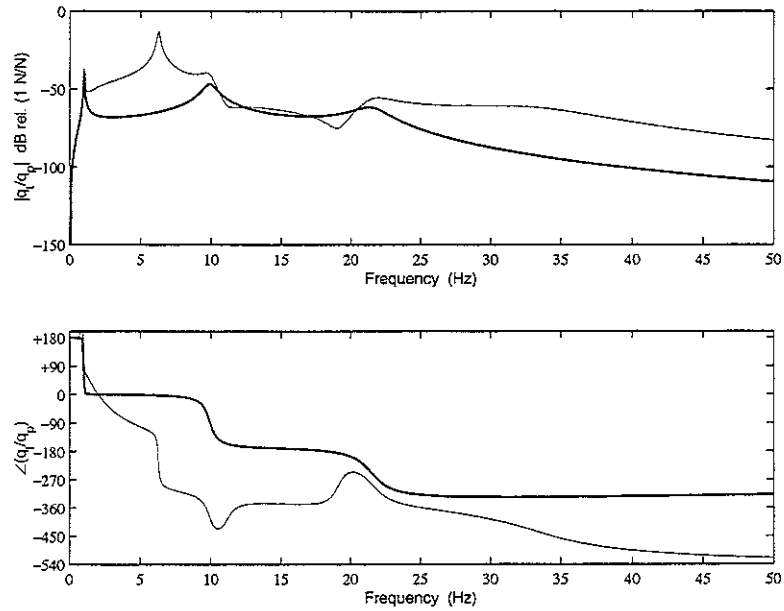

Fig. 53 *Bode plot of the transfer function between primary excitation and total force of the ideal system without control (solid line) and the realistic vibration isolation system (faint line) based the sum of integrated force and integrated velocity feedback control. Realistic electronic components are used, the time delay is assumed to be 0.001 seconds, the force feedback gain is 2, and the velocity feedback gain is 500.*

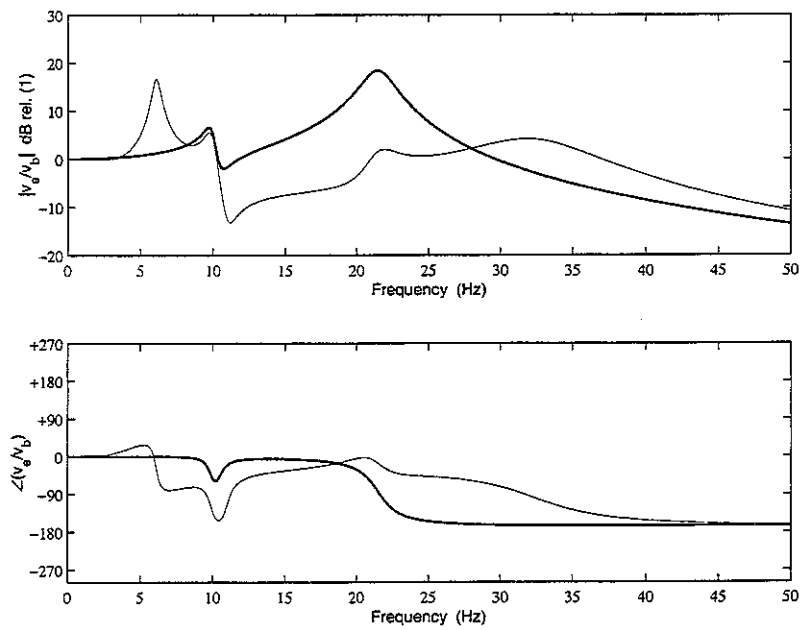

Fig. 54 *Transmissibility of the ideal system without control (solid line) and the realistic vibration isolation system (faint line) based on the sum of integrated force and integrated velocity feedback control. Realistic electronic components are used, the time delay is assumed to be 0.001 seconds, the force feedback gain is 2, and the velocity feedback gain is 500.*

2.8 Conclusions

Inertial actuators do not need to react off a base structure, so they can be used as modules that can be directly installed on a vibrating structure. This feature makes them very attractive.

A review of different strategies for active isolation using an inertial actuator was presented. For all of them, a matrix model has been used which assumes that the system is divided into four elements: base, passive mounts, equipment, and inertial actuator.

Feedback stability limits, performance, and robustness were considered for each case. In particular, once the theoretical analysis was completed, a realistic case using real commercial components was analysed. Table 1 shows the comparative results. In particular, the second and fourth columns report the maximum and average computed attenuation values for, respectively, the total force and the equipment velocity. The third and fifth columns show the frequency range within which the attenuations are effective. The judgement reported in the last column evaluates the robustness of the different control strategies when the aim is to minimize the equipment velocity.

Integrated velocity feedback control is unconditionally stable for an ideal system, while it is conditionally stable for real systems. The performance of an ideal integrated velocity feedback controller is good within a considerable frequency range. Its simplicity then makes this solution very attractive. Unfortunately high gains may be needed to obtain substantial attenuation and this is clearly a limit because in real systems high gains do not guarantee stability. However, the realistic analysed system was insufficiently robust, with performance limitations.

Force feedback control is unconditionally stable for an ideal system, while it is conditionally stable for real systems. Also for this case, possible instabilities may occur at low frequency. It is not appropriate to minimize the equipment velocity using this strategy, while, on the other hand, the performance of an ideal force feedback controller is very good if employed to reduce the transmitted force. Unfortunately, real systems seem to be poorly robust compared to the ideal case, therefore it is hard to obtain stable systems with high gains. In other words, high-end components are needed in order to use the good theoretical capabilities of this method. This is why the results on performance and robustness shown in Table 1 do not have to mislead.

Integrated force feedback control is unconditionally stable for an ideal system, while it is conditionally stable for real systems. Possible instabilities may occur especially at high frequency. The performance of a real integrated force feedback controller is very good, and its robustness is good, but only if the attenuation of the transmitted force is considered.

Finally, a combination of force-based and velocity-based feedback control laws was studied. First, the force and velocity feedback strategy was analysed. Being the system linear, the overall behaviour is the superposition of a force feedback controller and a velocity feedback controller. Ideal systems are conditionally stable, and real system may encounter low frequency stability problems, due to the electronics. This poses robustness problems that must be taken into account by the designer. The performance of the closed loop system greatly depends on the choice of the feedback gains. These aspects have been discussed. One of the main findings is that force feedback control (in ideal or semi-ideal systems) is able to stabilize systems that were unstable if only the velocity feedback controller was applied.

Then, the integrated force and velocity feedback strategy was analysed. Out of the 6 presented cases, this method showed an excellent robust behaviour and also good

performance. In addition, regarding the minimization of the equipment velocity, it was shown that the frequency range of interest in which the controller is effective is wider than in the other methods. Integrated force and velocity control is definitely a very interesting and very promising approach.
A combination of integrated force and integrated velocity offers a good robust behaviour and very good performance within the frequency range between the actuator natural frequency and the equipment natural frequency.

Feedback Controller	**Max/Ave Force Attenuation (dB)**	**Frequency range Force (Hz)**	**Max/Ave Velocity Attenuation (dB)**	**Frequency range Velocity (Hz)**	**Performance of the Realistic System**
DVFB	-/-	-	8/3	15-25	poor
Integrated Velocity	-/-	-	6/3	11-23	poor
Force	7/3	9.4-2000	amplification	11-22	poor
Integrated Force	33/8	3.1-2000	amplification	11-20	poor
Force + Velocity	6/2	10-11	8/4	18-25	poor
Intgrd. Force + Velocity	amplification	4-2000	22/9	12.5-2000	very good
Intgrd. Force + Intgrd.Vel.	amplification	2-2000	20/10	10-28	good

Table 1 *Performance and Robustness comparison of the control strategies applied to the same realistic electro-mechanical system.*

In this study it was assumed that the actuator resonance frequency was smaller than the equipment natural frequency. Appendix A reports the analysis of the opposite case. The main result that can be drawn from this study is that when the inertial actuator resonance frequency is greater than the equipment natural frequency, the overall system is more difficult to control and the control strategies here presented do not show good results. The best solution that was found was adopting a combination of force and integrated velocity.
When the break frequency of the actuator falls before the structural frequency and DVFB is implemented, the closed loop system is almost always unstable as shown by Zimmerman and Inman (1990.) This is due to the phase characteristics of the inertial actuator. When other strategies are implemented, including double loop feedback control, it was found that the performance of the overall system is not satisfactory. This is mainly due to the inherent dynamics of the inertial actuator, which was shown to be that of a high-pass filter whose characteristics are shaped by the spring and damper rates. In fact, the simplest way to describe the dynamics of the actuator is by its break frequency, which indicates the frequency at which the Bode magnitude plot of the inertial actuator breaks flat from a 40 dB/decade rise, and the phase plot goes through 90 degrees. In other words, the output force level is severely limited at frequencies below the break frequency, and those modes that fall below the break frequency cannot be effectively attenuated.

APPENDIX A: Equipment Isolation when the Inertial Actuator Resonance Frequency is greater than the Structural Frequency of Interest

When the inertial actuator resonance frequency is greater than the equipment natural frequency of interest, the overall system turns out to be more difficult to control, therefore, when possible, an actuator resonance frequency below the structural frequency is recommended (Zimmerman and Inman, 1990.)

In this study the actuator mass was changed to 0.5 kg, its stiffness was changed to 60000 N/m, and its damping to 10 Ns/m. This choice leads to an inertial actuator natural frequency of about 18.5 Hz and an equipment natural frequency of about 60.3 Hz.

When DVFB is used to control the equipment velocity, an additional phase shift due to the structure compromises the feedback stability. The Nyquist plot (Fig. a1) shows a portion of the curve at low frequency that lies in the negative real plane. In contrast to the corresponding case described in 2.1, the actuator acts at higher frequencies and it must be able to attenuate the behaviour of the equipment, which lies at lower frequencies.

When the feedback gain is set to 240, the stability limit is reached. In this configuration the closed loop behaviour shows good attenuation (15 dB maximum, 7 dB average) within 55 and 70 Hz, but, on the other hand, it shows a structural amplification between 16 and 19 Hz. This phenomenon, which can be up to 20 dB, is exactly the opposite of what we aimed. In other words, the inertial actuator is not able to be effective at frequencies below its own resonance frequency, where it turns out to be counterproductive.

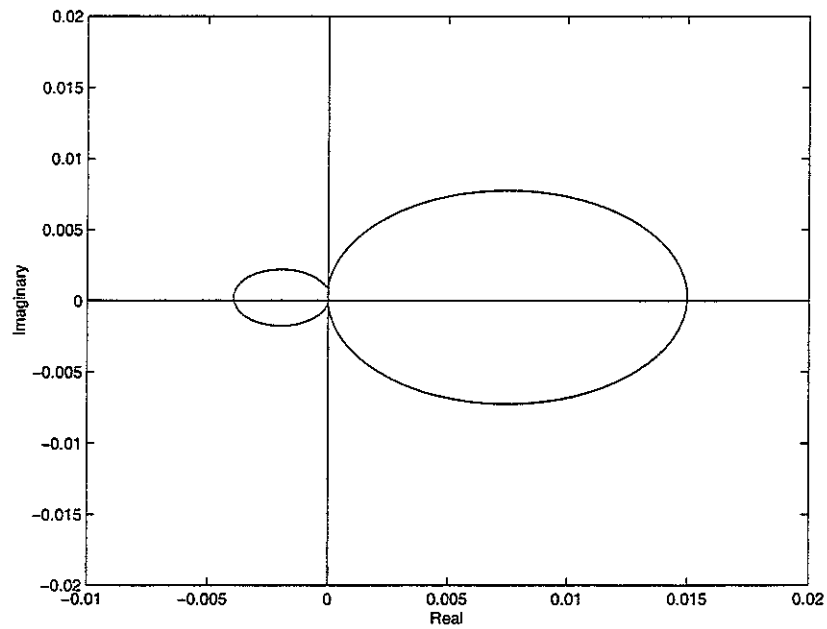

Fig. a1 *Nyquist plot of the transfer function between secondary excitation and equipment velocity of a vibration isolation system with an inertial actuator and velocity feedback control. ω varies from 0 to $+\infty$.*

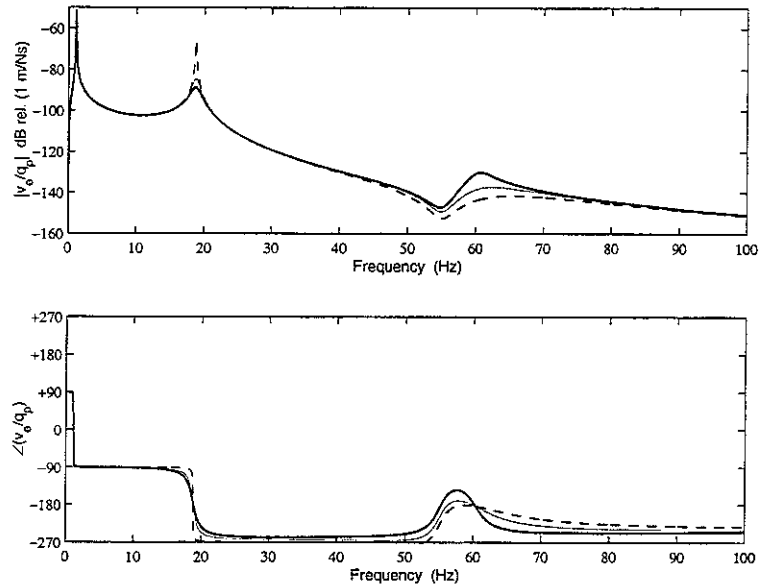

Fig. a2 *Bode plot of the transfer function between primary excitation and equipment velocity of a vibration isolation system with an inertial actuator and velocity feedback control. Velocity feedback gain h_v = 0 (bold line), h_v = 100 (faint line), h_v = 240 (dashed line.) This latter case causes closed loop system to be in its stability limit.*

When integrated velocity feedback is applied, the Nyquist plot is rotated by 90°, as described in 2.2. Also in this case poor performance and poor robustness are achieved for real systems. When force or integrated force are used as control strategy, the Nyquist plots remind of that ones that were obtained in 2.3 and 2.4. The shape is similar, but the behaviour is quite different, and the main reason is that this time the first loop that is travelled (increasing the frequency) is the inner loop, which describes the structure. Since this loop is small, large attenuations cannot be achieved. Moreover, attenuations in the transmitted force to the equipment can be obtained, while the equipment velocity either remains unchanged or it increases, defeating the purpose of the control system. Only force or integrated force control strategies are therefore ineffective or counterproductive in order to minimize the transmitted equipment velocity.

When multichannel control algorithms are implemented, the situation does not improve much. In general, attenuation in the transmitted force can be achieved, but amplification in the equipment velocity occurs, especially within a frequency range about the equipment mode. This is due to the fact that force is not sufficient in order to act effectively on the transmitted equipment velocity: velocity feedback is needed. On the other hand, the problem with velocity feedback is that the inner loop, which describes the structure, does not start with a vertical tangent, but shows a positive slope. Its shape is not entirely contained on the right hand side of the (1,0) point. By increasing the velocity gain, the inner loop expands and the values that it assumes nearby the equipment natural frequency are larger than without control. This causes the amplification effect.

The only promising case is when force and integrated velocity are applied. This strategy was the worst one in the previous analysis, while now it seems to be the only one that offers some results of interest. Figs. a3 and a4 report, respectively, the Nyquist plot and the close loop performance of this case. In particular, between 16 and 50 Hz, a maximum velocity attenuation of 15 dB (6 dB average) is shown. A velocity transmissibility analysis would lead to the same conclusions.

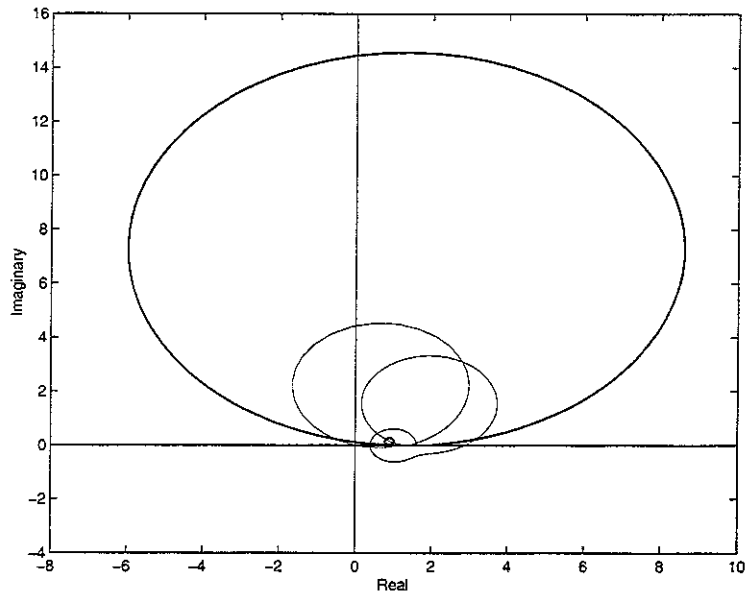

Fig. a3 *Multichannel Nyquist plot of the determinant of* $(\boldsymbol{I}+\boldsymbol{G}(j\omega)\boldsymbol{H}(j\omega))$. *The controller is the sum of force and integrated velocity feedback. The bold line shows the ideal model with double feedback, while in the faint line realistic electronic components are used, the time delay is assumed to be 0.001 seconds, the force feedback gain is 0.08, and the velocity feedback gain is 1110.* ω *varies from 0 to* $+\infty$.

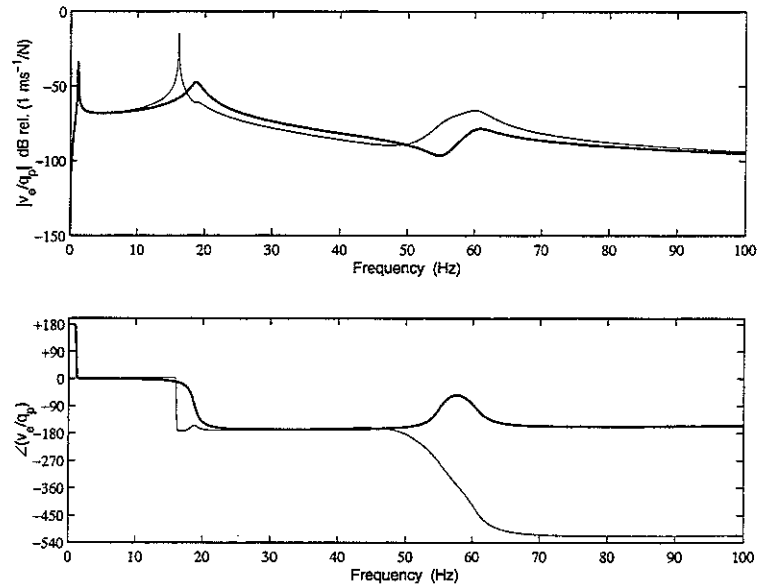

Fig. a4 *Bode plot of the transfer function between primary excitation and equipment velocity of the plant response (solid line) and the realistic vibration isolation system (faint line) with the sum of force and integrated velocity feedback control. Realistic electronic components are used, the time delay is assumed to be 0.001 seconds, the force feedback gain is set to 0.08, and the velocity feedback gain is set to 1110.*

References

Ananthaganeshan, K. A., Brennan, M. J., and Elliott, S. J., 2001, "Low and High Frequency Instabilities in Feedback Control of a Vibrating Single Degree of Freedom System," ISVR Technical Report No. 870.

Balas, M. J., 1978, "Direct Velocity Feedback Control of Large Space Structures," J. Guidance and Control, Vol. 2, No. 3, pp. 252-253.

Beard, A. M., von Flotow, A. H., and Schubert, D. W., 1994, "A Practical Product Implementation of an Active/Passive Vibration isolation System," *Proc. IUTAM Symposium on the Active Control of Vibration*, Bath, pp. 101-108.

Benassi, L., 2001, "Equipment Isolation of a SDOF System with an Inertial Actuator using Feedback Control Strategies – Part I: Theory," Internal Progress Report, ISVR, University of Southampton.

Bhat, S P., Tanake, M., and Miu, D. K., 1991, "Experiments on Point-to-Point Position Control of a Flexible Beam using Laplace Transform Technique - Part I: Open-Loop," Journal of Dynamic Systems, Measurement, and Control, Vol. 113, September, pp. 432-437.

Crede, C. E., and Ruzicka, J. E., 1996, "Theory of Vibration Isolation," Chapter 30, C. M. Harris, ed., *Shock and Vibration Handbook*, McGraw Hill, New York.

Elliott, S. J., Serrand, M., and Gardonio, P., 2001, "Feedback Stability Limits for Active Isolation Systems with Reactive and Inertial Actuators," J. Vibration and Acoustics, Vol. 123, April 2001, pp. 250-261.

Fuller, C. R., Elliott S. J., and Nelson, P. A., 1996, *Active Control of Vibration*, Academic Press.

Gardonio, P., Elliott, S. J., and Pinnington, R. J., 1997a, "Active Isolation of Structural Vibration on a Multiple-Degree-of-Freedom System, Part I: the Dynamics of the System," J. Sound and Vibration, **207**, No. 1, pp. 61-93.

Gardonio, P., Elliott, S. J., and Pinnington, R. J., 1997b, "Active Isolation of Structural Vibration on a Multiple-Degree-of-Freedom System, Part II: Effectiveness of Active Control Strategies," J. Sound and Vibration, **207**, No. 1, pp. 95-121.

Gardonio, P., Elliott, S. J., 1998, "Driving Point and Transfer Mobility Matrices for Thin Plates Excited in Flexure," ISVR Technical Report No. 227.

Howard, C. Q., Hansen, C. H., 1997, "Active Isolation of a Vibrating Mass," Acoustics Australia, Vol. 25, No. 2, pp. 65-67.

Karnopp, D., 1995, "Active and Semi-active Vibration Isolation," ASME J. Mech. Des., **117**, pp. 177-185.

Kim, S. M., Elliott, S. J., and Brennan, M. J., 1999, "Active Vibration Isolation of a 3-Dimensional Structure using Velocity Feedback Control," ISVR Technical Memorandum No. 845.

Miu, D. K., 1993, *Mechatronics*, Springer-Verlag.

Preumont, A., 1997, *Vibration Control of Active Structures*, Kluwer Academic Publishers.

Preumont, A., Francois, A, Bossens, F., Abu-Hanieh, A., 2001, "Force Feedback versus acceleration feedback in active vibration isolation," Manuscript submitted to *Journal of Sound and Vibration.*

Ren, M. Z., Seto, K., and Doi, F., 1997, "Feedback Structure-Borne Sound Control of a Flexible Plate with an Electromagnetic Actuator: the Phase Lag Problem," J. Sound and Vibration, **205**, No. 1, pp. 57-80.

Serrand, M., 1998, "Active Isolation of Base Vibration," MSc thesis, University of Southampton.

Serrand, M., and Elliott, S. J., 2000, "Multichannel Feedback Control for the Isolation of Base-Excited Vibration," J. Sound and Vibration, **234**, No. 4, pp. 681-704.

Ungar, E. E., 1992, "Vibration Isolation," Chapter 11, *Noise and Vibration Control Engineering*, L. Beranek and I. L. Ver, eds., Wiley, Chichester.

Zimmerman, D. C., and Inman, D. J., 1990, "On the Nature of the Interaction Between Structures and Proof-Mass Actuators," J. Guidance, Control, ad Dynamics, **13**, No. 1, pp. 82-88.